Space Weather®

RESEARCH ARTICLE
10.1029/2023SW003453

Mid-Latitude Double H-Spikes: Their Properties and Signatures in Different Geomagnetic Indices

E. Saiz[1], A. Guerrero[1], and C. Cid[1]

[1]Space Weather Research Group, Departamento de Física y Matemáticas, Universidad de Alcalá, Alcalá de Henares, Spain

Key Points:

- Mid-latitude ground magnetic disturbances observed as double H-spikes are remote effects of the field-aligned currents originated during substorms
- Double H-spikes pose a potential risk to damage technology, even located at midlatitudes, by generating geomagnetically induced currents
- SuperMAG SMR12 and SMR00 sector indices can monitor H-spikes for space weather purposes

Correspondence to:
E. Saiz,
elena.saiz@uah.es

Citation:
Saiz, E., Guerrero, A., & Cid, C. (2023). Mid-latitude double H-spikes: Their properties and signatures in different geomagnetic indices. *Space Weather*, *21*, e2023SW003453. https://doi.org/10.1029/2023SW003453

Received 6 FEB 2023
Accepted 15 MAY 2023

Abstract Proper assessment of geomagnetic disturbances is a key aspect of space weather as technology is often impacted by space weather activity without previous warnings or proper forecasts. Double H-spikes are a form of longitudinal asymmetry observed at midlatitudes. They are geomagnetic disturbances occurring simultaneously on the dayside and nightside as a negative/positive H-spike, which go unnoticed through common geomagnetic indices. This work presents the results of a systematic search for double H-spikes occurred over a 23-year period and analyzes characteristics of the double H-spikes such as the occurrence dependence on the solar cycle, season, intensity and phase of the geomagnetic storm. Our outcomes indicate that double H-spikes are a global phenomenon closely related with the substorm phenomenon and the ground magnetic disturbances observed at mid-latitude are remote effects of field-aligned currents (FACs). FACs would be the part of the substorm current wedge developed from the expansion onset of intense substorms whose effects have wide longitudinal extend as they are observed on the dayside and the nightside. Also mid-latitude global SYM and ASY indices are affected by FACs during those periods. Time derivatives of the SuperMAG SMR12 and SMR00 sector indices allow us to conclude that double H-spikes, as short-time high-intensity magnetic disturbances, pose a potential risk to damage ground-technological systems at midlatitudes.

Plain Language Summary Space weather plays an important role in the impacts to society by natural sources. Technology is still frequently impacted by Solar activity without proper warnings. It is clear that scientists and institutions are missing some aspects of the physics governing some of these events. In previous works, double H-spikes have been related to the most dangerous space weather events in history and also proven to go unnoticed by the traditional indicators used by the community. In this work we present new features like their distribution of occurrence, their intensities and their link to higher magnetic latitude activity. We show that this link is one of the reasons for the significant threat posed by H-spikes but also the key feature to detect them. Their identification will also help in forecasts and release of warnings by responsible centers and institutions.

1. Introduction

The research of geomagnetic disturbances plays an important role in the analysis and assessment of the impacts that the Sun has on technology and society. Recent results established the importance of evaluating local geomagnetic records and the role of local geomagnetic indices when assessing extreme space weather events like the Carrington or the Halloween geomagnetic storms (Cid et al., 2014, 2015; Saiz et al., 2016, 2021). These results gave evidence of a certain type of geomagnetic disturbances (the H-spikes) not previously recognized as hazardous to technology and has been analyzed in the literature as part of other topics of interest. This might have been due to a lack of perspective of the phenomenon associated with this type of magnetic disturbances, both in its temporal and spatial scale.

The H-spikes are identified in the horizontal component of the ground magnetic field recorded by mid-latitude magnetic stations. They are bay-like disturbances of short-time (~1.5–2 hr) and considerable intensity (>100 nT) that occur at the same UT time at locations of the world almost longitudinally opposite to each other. While a positive bay takes place at stations located on the nightside, a negative bay occurs at stations located on the dayside, thus labeled as double H-spikes. The left picture in Figure 1 shows a sketch of a double H-spike, which corresponds to the horizontal component as recorded by two stations located on the dayside (red) and nightside (blue). Note that the black line in the sketch, indicating the longitudinally averaged magnetic disturbance, misses information on such an important magnetic disturbance. The panel on the right is an overlapping stack plot of the magnetograms for the N component of 13 ground-based magnetometers, all located at a similar magnetic

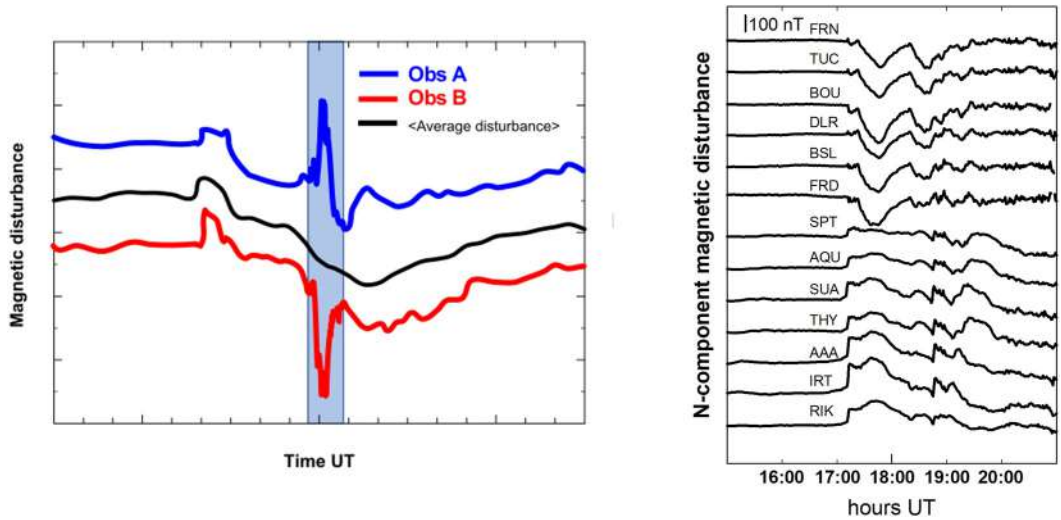

Figure 1. (left) Typical pattern of a double H-spike as observed at two midlatitude stations: Obs A, at the night sector, and Obs B, at the day sector. The black line in the sketch corresponds to the longitudinally averaged magnetic disturbance, similar to what global indices such as Dst or SYM-H perform. Blue shadowed area indicates the time interval when the double H-spike occurs. (right) Stack plot of the N-component magnetograms (baseline subtracted by SuperMAG tool) recorded at mid-latitude stations on 21 January 2005 between 15:00 UT and 21:00 UT. The stations are located at similar magnetic latitude (~40°N) and longitudinally spread. The name of each station is the IAGA code. A double H-spike occurs since ~17:20 UT to 18:20 UT when the stations located at the dayside (nightside) magnetic local times sectors record a negative (positive) H-spike.

mid-latitude but spread in longitude. It shows a double H-spike occurred on 21 January 2005. In the time interval from about 17:20 UT to 18:20 UT, the stations at the bottom half from AQU to RIK (at the nightside magnetic local time (MLT) sectors) show the disturbance as a positive bay while the top half of the stations from FRN to FRD (at dayside MLT sectors) show the disturbance as a negative bay.

Nighttime positive bays and daytime negative bays have been treated previously in literature, but only as two independent features without remarking their simultaneity on time. The positive magnetic bay at midlatitude magnetometers has been related to the expansion of magnetospheric substorms (Akasofu, 1964). Their effects are caused by the equivalent electrical current system named the substorm current wedge (SCW) (McPherron et al., 1973; Pytte et al., 1976). The model of the SCW, as a simplified representation of the current system associated with substorms, consists of a single loop formed by four line currents. Two of them follow the path marked by geomagnetic field lines (field-aligned currents, FACs), one flowing into the ionosphere and the other one flowing out of the ionosphere. The other two connect them together. One is a line current flowing westward on the ionosphere and the other one is part of the magnetospheric line current. The FACs play an important role in the coupling between the magnetosphere and the ionosphere (e.g., Siscoe et al., 1991). The directions of these FACs are the same as for the large-scale region-1 system (Iijima & Potemra, 1976), that is, the upward FAC is localized in the premidnight sector while the downward FAC is more broadly azimuthally distributed along the auroral oval post-midnight (Untiedt & Baumjohann, 1993).

While the SCW begins to flow at the onset of the substorm, and persists for somewhat less than an hour, the large scale pattern of the SCW in the midlatitude magnetic field has a distinctive pattern. Midlatitude stations are far from wedge currents and therefore measure a net effect of the currents of the system that make up the SCW rather than local details (Kepko et al., 2015). According to the Biot-Savart law, everywhere within the wedge, the north component (or H component) is positive and symmetric about the central meridian. Likewise, Kepko et al. (2015) show that the wedge may form almost anywhere in the night sector and may be narrow or as large as the entire nighttime sector.

The clear feature of a positive bay seen at midlatitudes at the night sectors was suggested as a good indicator of substorm onset because it is simultaneous to the auroral expansion, and less susceptible to interfere with the small scale features of the electrojet. In fact, the Midlatitude Positive Bay (MPB) index (McPherron & Chu, 2017) has been designed recently to quantify the strength of the magnetic perturbations caused by the SCW. The index is

derived from midlatitude magnetometers located on the nightside of the Earth and is considered as a proxy for the substorm onsets because the MPB onsets are closely associated with the auroral expansion onsets (McPherron & Chu, 2018).

New multi-spacecraft missions such as Cluster (Escoubet et al., 2001), THEMIS (Time History of Events in the magnetosphere-Ionosphere System) (Angelopoulos, 2008), Swarm (Friis-Christensen et al., 2006), and MMS (Magnetospheric MultiScale) (Burch et al., 2016) have added considerable observational knowledge, allowing to understand the structure and dynamics of magnetospheric current systems around Earth (see e.g., Ganushkina et al., 2015; Ganushkina et al., 2018, and references therein), especially on the important role of fast flows in producing the stresses that generate the SCW. The AMPERE (Active Magnetosphere and Planetary Electrodynamics Response Experiments) project was conceived to investigate the dynamic of FACs (see Coxon et al. (2014) for a review). AMPERE provides global FAC measurements which, along with large integrated networks of radars, all-sky imager data, and numerical techniques to generate equivalent current maps, reconfirm the original SCW picture although in many cases the system is more complicated that the simple picture (see Kepko et al. (2015) for a recent review about the historical development of the SCW).

Negative magnetic bays on the dayside at equatorial latitudes associated with substorms have been reported in the literature (Kikuchi et al., 2000; Sastri et al., 2001). Coherently with the negative bay at high-latitude stations, the bay amplitude decreases with the latitude but it is amplified at the daytime dip equator compared to the low-latitude negative bay. The negative bay-like disturbance, starting at the onset of expansion phase activity, is explained as result of the prompt penetration of the convection electric field into the equator causing a large-amplitude negative deflection at dip equator. The enhanced amplitude at the daytime dip equator compared with stations away from the equatorial electrojet influence has been attributed to a significant contribution of the ionospheric currents to the negative bay effect in the H component (Sastri et al., 2001).

However, the negative magnetic bay at mid and low latitudes in the afternoon sector like the positive magnetic bay in the midnight and morning sectors, with monotonic decrease of amplitude from midlatitudes to the equator, have been generally understood in terms of the three-dimensional current system in the magnetosphere of the SCW (Kamide & Fukushima, 1972; Reddy et al., 1988). The bays are thus perceived as being primarily due to distant currents, namely, the FACs, partial ring current (PRC) and cross-tail current, where at midlatitudes the FAC effects could be dominant, outweighing the effects of ionospheric currents (e.g., Kikuchi et al., 2001).

Saiz et al. (2021) set the double H-spikes in the context of geomagnetic indices commonly used for quantifying ground magnetic perturbations recorded at low-latitudes and high-latitudes. Specifically, they searched for events of large longitudinal asymmetry observed at midlatitude stations (~40°N magnetic latitude), which occurred during extreme events, where an event was considered extreme when the Dst and AL indices exceeded the thresholds Dst ≤ -200 nT and AL $\leq -2{,}000$ nT respectively. Their results evidenced that by using only global indices there is a risk of missing the detection and monitoring of this kind of significant magnetic disturbances during extreme geomagnetic storms.

In the present work we come back to double H-spikes, but getting deeper into their characteristics. Our goal is to answer questions such as: do they occur only during extreme storms?; how frequent are double H-spikes at midlatitudes?; do they occur in a specific storm-time phase or even out of storm-time, during quiet geomagnetic activity level?; what is the global geomagnetic perspective of the ground magnetic disturbances during their occurrence?; how are the double H-spikes related to other magnetospheric phenomena, such as substorms?; which current system is most likely responsible for those midlatitude magnetic perturbations?; do they pose a risk to create geomagnetically induced currents (GICs) during their occurrence?

GICs are one of the potentially dangerous features of space weather, which can lead to malfunctions and blackouts of the electric power transmission networks. GICs are induced in long conducting infrastructures by rapid fluctuations in the magnetic field (e.g., Schillings et al., 2022; Wik et al., 2009). Therefore, double H-spike events appear as a hazard for GICs, with the potential to create significant geoelectrics fields and hence to drive GICs at midlatitude zones. Thus answering all the questions above will help to understand this kind of magnetic disturbances, and will provide a first approach to its potential impact at midlatitude to generate GICs, which could feed into future impact studies at those latitudes.

In Section 2 we describe the method of systematic search used to detect the double H-spike events from a wider perspective than in our previous works. In this Section we also obtain the occurrence statistical distributions and

make a selection of events as case studies for a deeper analysis. Then, in Section 3 we analyze the response of the RC and the auroral electrojets during the selected double H-spikes events by using the nominally representative magnetic indices of those currents. Section 4 is dedicated to show the close relationship between double H-spike events and the substorm phenomenon. The double H-spike events that occurred during non-storm time are analyzed in Section 5, and some of the events that occurred during geomagnetic storms and were previously studied in the literature are analyzed in Section 6. We dedicate Section 7 to show the potential risk of the double H-spikes for driving GICs at midlatitude. Finally, in Section 8 we summarize our conclusions presenting answers to the raised questions.

2. Double H-Spikes at Midlatitudes

We have used SuperMAG geomagnetic indices (https://suermag.jhuapl.edu) for a systematic search of double H-spike events. Although at present time they are not endorsed by IAGA, we consider these indices the best option for such a search because of the use of a great number of stations, which reduces the number of spatial gaps to a minimum. These geomagnetic indices and others cited in this work are summarized in Table 3. Specifically, we focus on the SMR indices, derived by Newell and Gjerloev (2012) to quantify the global disturbances at mid latitudes. They are based on a method similar to that used to obtain the SYM-H index. Within the SMR indices there are four sector SMR-LT indices (LT indicating the hour representing the sector) and their average is the SMR index (symmetric RC index). Specifically, SMR-12 is defined as the average at each moment of time of the N component for all available ground magnetometer stations at magnetic latitudes located between −50° and +50° within the local time sector 09 MLT to 15 MLT and likewise the SMR-00 index is created from stations located within the local time sector 21 MLT to 03 MLT. We have chosen the SMR12 and SMR00 sector indices because they take into account the local character and the MLT distribution that are present during the double H-spikes (see sketch in Figure 1). Indeed, among the four possible sector indices, only the SMR12 and SMR00 indices can clearly and unambiguously show the day-night longitudinal asymmetry indicated by Saiz et al. (2021): the SMR12 index guarantees the disclosure of negative bays recorded at stations within the 09–15 MLT sector, while the use of SMR00 index guarantees the disclosure of positive bays recorded at stations within the 21-03 MLT sector.

In addition, the large number, approximately 100 stations, participating in the derivation of these indices, provides reliability and robustness to the geomagnetic disturbances provided by these indices (including their positive or negative signs).

Finally, before entering in the subsections we would like to note that the default coordinate system used by SuperMAGis slightly different from the usual HDZ coordinate system but has no influence on the current work. The SuperMAG coordinate system is the NEZ, where N is positive in the direction of the local magnetic north, E is positive in the local magnetic east direction and Z is positive in the vertical downward direction. These local references are obtained using a baseline obtained with the SuperMAG technique and they are expected to have very slow variations. Consequently, for the practical purposes of this paper, the disturbance field of the H (horizontal) component of the geomagnetic field can be regarded as the disturbance field of the N (northward) component in the coordinate system used in SuperMAG (Gjerloev, 2012). Therefore throughout this work we will continue using the terms H-spike and double H-spike, in spite of we will use the N component (via SMR12 and SMR00 indices) for systematic identification of the events.

2.1. Detection of Double H-Spike Events

To quantify the day-night longitudinal asymmetry of the H component at midlatitudes in form of a double H-spike we define the following index:

$$Range(t) = SMR00(t) - SMR12(t) \quad (1)$$

A systematic search to identify the periods where the condition $\text{Range}_{peak} \geq 150$ nT is fulfilled provides the list of double-spike events. The study period covers the years from 1998 to 2020. As the sign of the H-spike should be positive on the nightside and negative on the dayside, the identification of a double H-spike has been established with a positive threshold for the *Range* index, specifically 150 nT. A total number of 45 events has been obtained for the 23-years period (see Table 1). Each event is characterized by its intensity, the peak value

Table 1
List of Double H-Spike Events With Intensity Range$_{peak}$ ≥ 150 nT That Occurred Between 1998 and 2020

Year	Date (mm/dd hh:mm)	Doy	Range$_{peak}$ (nT)	Spikes ratio (±)	Phase of the storm	Dst$_{peak}$ (nT/class)
1998	05/04 03:25	124.1424	166.5	1.4	Late main phase	−205/intense
1998	08/27 08:16	239.3444	169.4	1	Late main phase	−155/intense
1998	09/25 06:36	268.2750	320.3	1.4	Late main phase	−207/intense
1999	09/22 21:35	265.8993	175.2	1.5	Late main phase	−173/intense
2000	07/15 17:06	197.7125	199.1	0.4	Early main phase	−300/extreme
2000	08/12 03:41	225.1535	187.8	0.7	Early main phase	−234/intense
2000	09/17 21:36	261.9000	295.8	1.9	Late main phase	−201/intense
2001	03/20 14:22	79.5986	160.7	2.8	Early recovery phase	−149/intense
2001	03/31 18:21	90.7646	156.3	1	Early recovery phase	−387/extreme
2001	04/08 20:58	98.8736	188.2	1.4	Middle main phase	−63/moderate
2001	04/11 16:12	101.675	298.3	1	Early main phase	−271/extreme
2001	04/13 10:33	103.4396	183.5	0.9	Late recovery phase	−271/extreme
2003	03/17 21:21	76.8896	157.3	1.8	PLA[a]	−40/low
2003	05/29 19:13	149.8007	231.2	1	Middle main phase	−144/intense
2003	08/18 07:15	230.3021	151.2	2.2	Middle main phase	−148/intense
2003	10/29 06:58	302.2903	681.8	0.8	Early main phase	−353/extreme
2003	10/29 23:14	302.9681	249.3	1.7	Late main phase	−353/extreme
2003	10/30 17:39	303.7354	196.6	1.3	Late recovery phase	−353/extreme
2003	10/30 19:56	303.8306	349.2	0.6	Early main phase	−383/extreme
2003	11/06 20:15	310.8438	160.5	1.3	PLA[a]	−10/low
2003	11/13 12:20	317.5139	156.1	1.1	PLA[a]	−25/low
2003	11/20 16:51	324.7021	156.8	1.1	Middle main phase	−422/extreme
2004	01/22 11:58	22.4986	155.4	1.1	Late main phase	−130/intense
2004	07/25 09:53	207.4118	167.4	0.8	Late main phase	−136/intense
2004	07/25 10:27	207.4354	165.3	1.1	Late main phase	−136/intense
2004	07/26 23:26	208.9764	232.3	0.9	Early main phase	−170/intense
2004	07/27 07:16	209.3028	176.8	1.3	Middle main phase	−170/intense
2004	07/27 09:18	209.3875	264.7	0.8	Late main phase	−170/intense
2004	11/08 01:27	313.0604	181.8	0.9	Middle main phase	−374/extreme
2004	11/09 20:10	314.8403	157.1	0.4	Middle main phase	−263/extreme
2004	11/09 20:37	314.859	262.2	0.8	Middle main phase	−263/extreme
2004	11/10 07:33	315.3146	182.6	2	Late main phase	−263/extreme
2004	11/10 08:29	315.3535	211.1	0.7	Late main phase	−263/extreme
2005	01/07 23:05	7.9618	316.7	1.6	Late main phase	−93/moderate
2005	01/18 08:04	18.3361	196.9	0.8	Late main phase	−103/intense
2005	01/21 17:50	21.7431	234.6	1	Early main phase	−97/moderate
2005	08/24 10:36	236.4417	385.4	0.6	Late main phase	−184/intense
2005	09/11 06:39	254.2771	166.9	0.8	Late main phase	−139/intense
2005	09/12 23:45	255.9896	198.5	2.4	Late recovery phase	−139/intense
2006	12/14 23:56	348.9972	247.1	1.6	Middle main phase	−162/intense
2006	12/15 12:14	349.5097	151.8	1.5	Early recovery phase	−162/intense
2010	04/05 09:26	95.3931	170.9	0.7	Early main phase	−81/moderate
2016	05/09 00:01	130.0007	150.3	1	Early recovery phase	−88/moderate

Table 1
Continued

Year	Date (mm/dd hh:mm)	Doy	$Range_{peak}$ (nT)	Spikes ratio (±)	Phase of the storm	Dst_{peak} (nT/class)
2017	03/27 20:05	86.8368	193.2	0.9	Early recovery phase	−70/moderate
2017	09/07 23:27	250.9771	252.8	1.1	Middle main phase	−122/intense

Note. The list provides information on: the year (column 1); the time when $Range_{peak}$ is reached in both mm/dd hh:mm UT and DoY formats (columns 2 and 3 respectively); the intensity of the double H-spike event (column 4); the strength ratio (column 5) of the two H-spikes contributing to the double H-spike (negative spike relative to the positive one); in which stage of the magnetic storm it takes place (column 6); the intensity of the magnetic storm, as seen by Dst_{peak}, and its category (column 7).

[a]PLA, Prolonged Low Activity.

of *Range*(*t*) (column 4), and its time of occurrence, that is, the time in which that peak value is reached (columns 2 and 3). Columns 5 to 7 provide additional information on the double H-spike events. Column 5 gives the strength ratio of both H-spikes (negative spike relative to the positive one). Note that a ratio >1 (<1) means that the positive spike has larger (smaller) strength than the negative one. The next column gives information on the phase of the geomagnetic storm when the double H-spike occurs (see Section 2.2 for our classification into early-, middle- and late-main phase); when happening within the first 5 hr after the Dst_{peak} value, the event is marked as early-recovery phase. In case the double H-spike event occurs just after a previous time interval kept for at least 10 hr of low activity ($Dst \geq -50$ nT), then we consider it as a non-storm time event, and it is named as Prolonged Low Activity (PLA). Column 7 includes the intensity of the geomagnetic storm during which the double H-spike takes place. The intensity of the storm is seen by the Dst_{peak} value, and its classification by intensity is defined in Gonzalez et al. (1994) and Echer et al. (2008) (moderate, intense, super-intense or extreme). In the case of the PLA events the value given is the average value of Dst in those previous 10 hr. Despite we have used the 1 hr Dst index following standard classification criteria, in the following we will use higher time-resolution (1 min) SYM and ASY data to make a better comparative of the instantaneous geomagnetic conditions at different latitudinal ranges (see Section 3).

2.2. Statistical Distribution of Double H-Spike Events

Figure 2 summarizes the statistical distribution of all double H-spike events detected during the interval of study from 1998 to 2020 (Table 1). Panels show the distribution dependence on year, season, level of magnetic activity when taking place, and their intensity.

Regarding the annual distribution, the sample is biased, according to the Pearson's chi-squared test, at a significance level of 99.9%. Panel (a) clearly shows that the number of events is concentrated in the Solar Cycle 23, specifically in its declining phase (years 2003–2005), probably corresponding to the higher intensity of Solar Cycle 23 compared to Solar Cycle 24. Minima of event occurrence are at solar minimum (years 2006–2010 and 2018–2020) and maxima are shifted about 3 years from the sunspot maxima. On the other hand, the high occurrence rate in the declining phase might be related to the presence of high speed streams (Borovsky & Yakymenko, 2017; Tanskanen et al., 2005).

The distribution of the number of events by seasons appears in panel (b). Seasons of the year in the Northern Hemisphere were considered: winter (December–January–February), spring (March–April–May) and so on. The number of events is greater in summer and fall compared to that in spring and winter, 28 events versus 17 events respectively. Nevertheless, when grouped into events occurring during equinoxes and solstices, they have a very similar distribution (24 events vs. 21 events respectively). The relative uniformity of occurrence throughout the year might indicate a seasonal non-dependence. Indeed a Pearson's chi-square of 3.98 provides a significance level of 74%, well below the 90% level required for statistical significance.

Panel (c) shows the occurrence distribution of this kind of events at different stages of the development of a geomagnetic storm. The classification into early-, middle- or late-main phase has been made dividing in three parts the time of duration of the main phase of the storm (time interval from the storm sudden commencement (SSC) to the peak value of the Dst index). If they occur after Dst_{peak}, then the double H-spike is considered an event occurred in the recovery phase of the storm. Specifically, panel (c) in Figure 2 shows that the largest number

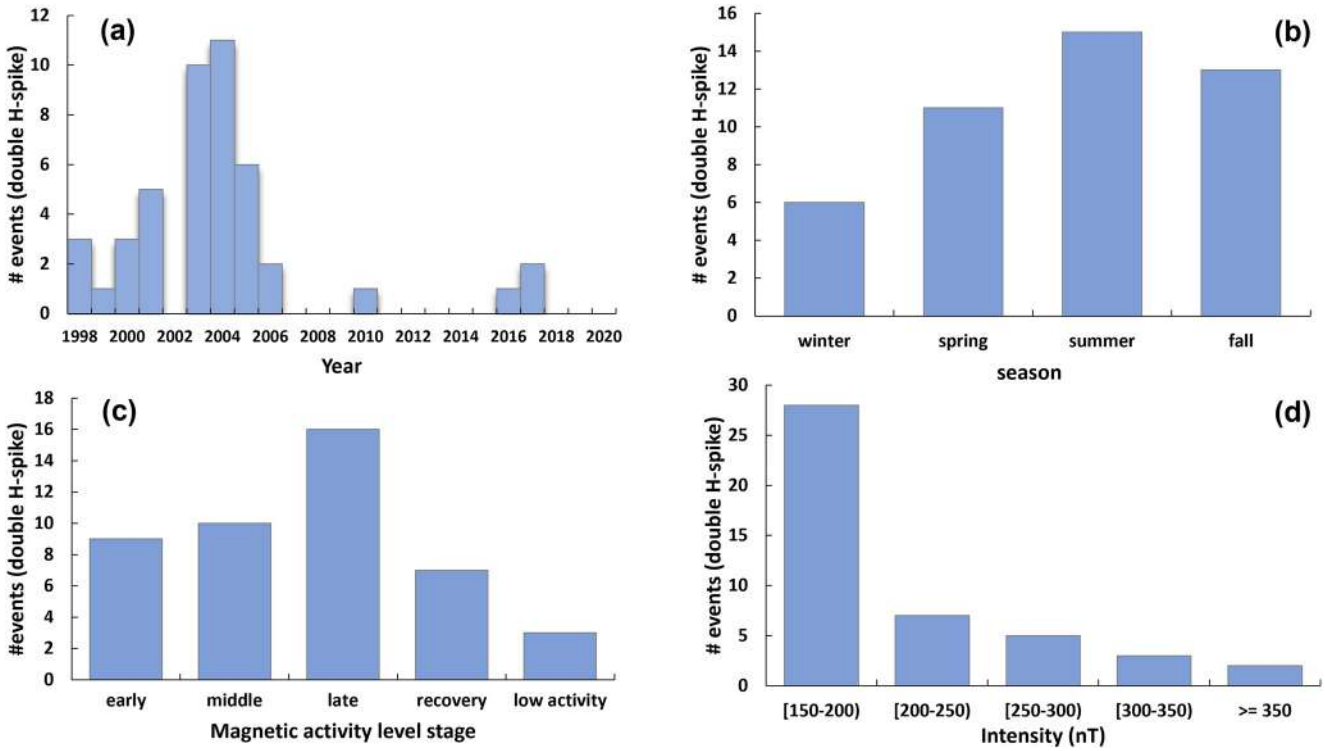

Figure 2. The four panels show the statistical distribution of the number of double H-spike events (Table 1) as a function of different variables. The upper panels correspond to the annual (a) and seasonal (b) distributions; the bottom panels correspond to the distribution of events according to the magnetic activity stage when they occur (c), and according to their intensity (d).

of double H-spike events is concentrated into the late-main phase (16), that is, in the last third of the time of the main phase of the storm, while the number of those that take place during the first and second third is comparable to the average (9). Note that a few number of events (3) occurred out of storm-time (orange bar) (in Section 5 we analyze this in more detail). The sample is clearly biased, with many more double H-spikes taking place during storm time than quiet time. If we exclude the PLA cases focusing only on the cases covering the four storm stages, the confidence is 77%, according to the Pearson's chi-squared test. Thus, there is no statistical evidence for the occurrence of the double H-spikes to vary with storm phase, but there is statistical evidence that they are less likely during low or quiet geomagnetic activity periods.

Panel (d) in Figure 2 shows the distribution of the number of events occurred within a range of intensity. As we can see, the intensity of most events is in the (150, 200) nT range. In fact, in the analyzed 23-year period, 10 events have intensities greater than 250 nT. Moreover, the number of events decays exponentially with increasing intensity (correlation factor $R = 0.98$). Only two double H-spike events exceeded 350 nT in the 23-year period: on 29 October 2003, in the early-main phase ($\text{Range}_{peak} = 682$ nT), and on 25 August 2005 in the late-main phase ($\text{Range}_{peak} = 385$ nT).

Other characteristics can be obtained from Table 1, specifically from the information given in columns 5 and 7. Indeed, the positive H-spike strength exceeds the negative one (ratio > 1) in 22 events. It is identical in 6 events, and lower (ratio < 1) in the remaining 17 events. This result suggests that there is no predominant trend of higher intensity observed in the H-spikes on the nightside compared to those on the dayside and vice versa.

Regarding the occurrence frequency of double H-spike events according to the intensity of the geomagnetic storm in which they take place, they are sorted in descending order as follows: 49% during intense storms (-250 nT $\leq \text{Dst}_{peak} \leq -100$ nT), followed by 31% during extreme storms ($\text{Dst}_{peak} < -250$ nT), and 13% during moderate (-50 nT $\leq \text{Dst}_{peak} \leq -100$ nT), and only 7% in non-storm time ($\text{Dst} > -50$ nT). These percentages are very similar to those found by Hajra et al. (2016), who studied extreme substorms (SSS) that occurred during the period 1981–2012: 46% were associated with intense storms, 49% with superstorms (extreme in our study), 1% with moderate storms and 4% occurred during geomagnetically quiet conditions.

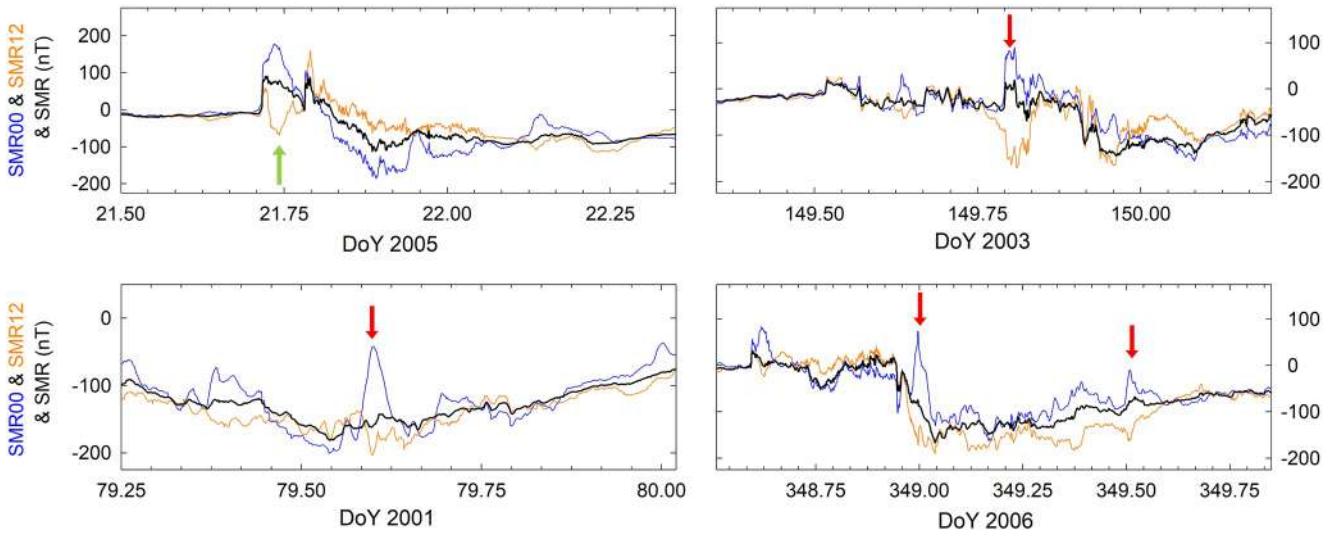

Figure 3. Examples of double H-spikes events which are not selected as case studies (plots with red arrows) and those which are (plot with a green arrow).

2.3. Selection of Double H-Spike Events as Case Studies

With the objective of going beyond a mere statistical analysis and getting some insights about the relationship of these events with the already known ionosphere/magnetosphere phenomenology and/or their possible sources, we select a subset of double H-spikes events that would be considered as case studies. For this task, we make a visual inspection of the full sample of double H-spike events (those listed in Table 1), looking for the three following features (to be considered as a case study all three must be met):

(a) prior to the double H-spike onset, the deviation of the value of SMR00 respect to that of SMR12 should not exceed about 20 nT;
(b) the overall pattern of activity in the SMR00 and SMR12 indices during the double H-spike interval should be smooth;
(c) the two H-spikes of the event, the positive and the negative, should have comparable strength, being no more than twice the one to the other (spikes ratio between 0.5 and 2.0).

These criteria are set with the objective to isolate the double H-spike events from other possible contributions from different sources and therefore be able to conclude without ambiguity about the source of the double H-spike phenomenology.

Figure 3 shows four plots with examples of double H-spike events. The event marked with a green arrow (top left panel) corresponds to an event chosen as a case study; the other events, marked with red arrows, correspond to events not selected as case studies. The bottom left and the top right plots are examples where at least one of the criteria (a, b, or c) is not met. Indeed, the bottom left plot shows that during the event the positive spike strength, seen in SMR00 (blue line), is much larger than that of the negative spike, seen in SMR12 (orange line) (spikes ratio = 2.8, Table 1); the event of the top right plot shows a negative H-spike profile seen in SMR12 which is not smooth, together with a significant deviation in both indices when the enhancement begins. Analogously, the bottom right plot shows two events, the first presents a complex development of the disturbances (criterion b not met) and an important asymmetry in strength (criterion c not met); on the other hand, the second event marked in the panel also has a large deviation in the sector indices when the double H-spike begins (criterion a not met).

Following the aforementioned criteria to select a double H-spike event as case study, we obtained a total of 12 events to be considered as case studies as listed in Table 2.

We can see that 7 out of the 12 events (58%) have a Range_{peak} intensity greater than 200 nT although this feature was not part of the criteria to select events as case study. It is also remarkable the diversity in the stage of the geomagnetic storm where the double H-spike events occur (see columns 5 and 6 in Table 2).

Table 2
List of the Double H-Spike Events Selected as Case Studies

Event	Date (yyyy/mm/dd hh:mm)	DoY	$Range_{peak}$ (nT)	Phase of the storm	Dst_{peak} (nT)/class
#1	1998/09/25 06:36	268.2750	320	Late	−202/intense
#2	2000/09/17 21:36	261.9000	296	Middle	−201/intense
#3	2001/04/08 20:58	98.8736	188	Middle	−63/moderate
#4	2001/04/11 16:12	101.6750	298	Early	−271/extreme
#5	2003/03/17 21:21	76.8896	157	PLA[a]	−40/low
#6	2003/10/29 06:58	302.2903	682	Early	−353/extreme
#7	2003/11/06 20:15	310.8438	161	PLA[a]	−10/low
#8	2005/01/07 23:05	7.9618	317	Late	−93/moderate
#9	2005/01/21 17:50	21.7431	235	Early	−97/moderate
#10	2005/08/24 10:36	236.4417	385	Late	−184/intense
#11	2010/04/05 09:26	95.3931	171	Early	−81/moderate
#12	2017/03/27 20:05	86.8368	193	Early recovery	−70/moderate

Note. The complete information about each of the events can be found in Table 1.
[a]PLA, Prolonged Low Activity.

3. The Double H-Spike Disturbances in a Global Magnetic Scenario

With the objective to study the relationships of the events with a physical phenomenon and/or a certain class of magnetic effect, we will analyze the features emerging on other geomagnetic indices providing a first discussion of the nature of the double H-spikes and its possible associated current system. We will address this discussion by outlining what is known of correlations/associations between the global indices indicative of the auroral electrojet currents and the asymmetric/symmetric elements of the RC. These first results will lay foundations for the discussion of the physical phenomenon of substorms in the next Section.

While global geomagnetic indices are not particularly useful for looking into specific processes or for justifying decision making at the local level, they can be very helpful in understanding general activity levels in different regions of geospace (Liemohn et al., 2018). They are well known to be indicators of large-scale currents that take part in the magnetosphere-ionosphere coupling. In this scenario, and with the aim of having a global perspective about the ground magnetic field responses during a double H-spike event, we will consider in this paper high-latitude and mid-(low-)latitude indices. In order to facilitate the reading throughout the paper Table 3 gives an overview of the indices. The 'global' character of an index in column 4 refers to the involvement of magnetometer stations covering 360° in longitude to obtain the index.

As proxies for the high-latitude ground magnetic activity level, we use the SuperMAG SML and SMU indices. The SML and SMU indices (Newell & Gjerloev, 2011a, 2011b) are typically derived from approximately 110 stations located at geomagnetic latitudes between 40° and 80°. They reflect the westward and eastward auroral electrojets respectively. The procedure to derive these indices is based on the same method as obtaining the auroral AL and AU indices. Thus, SML and SMU are obtained from the envelopes (the lower and upper one respectively) of the N (North) component of the ground geomagnetic field after removing the baseline. The greater latitudinal range and, consequently, the greater number of observatories used for their derivation (vs. the 12 stations used in the derivation of the AE indices) has the advantage not to miss high-latitude geomagnetic activity even when the auroral oval expands toward the equator during geomagnetic storms.

It is well known that at mid- (low-) latitude the disturbance of the magnetic field is not axially symmetric, especially during the development of a geomagnetic storm, where the contribution of the asymmetric part can be even greater than the symmetric one (Akasofu & Chapman, 1964; Sugiura & Chapman, 1960). In regard to this, in order to study the symmetry during the events, we will use the high-resolution SYM and ASY indices (defined for both the H and D components of the geomagnetic field), which were conceived as indicators of the longitudinally symmetric (SYM-H and SYM-D) and asymmetric (ASY-H and ASY-D) disturbance field at midlatitudes. It has been extensively assumed that while SYM-H describes considerably well the effects of the symmetric part

Space Weather

10.1029/2023SW003453

Table 3
Summary of the Geomagnetic Indices Used or Cited in the Paper

Latitude zone	Geomagnetic index	Temporal resolution	Longitudinal range	# Of stations [lat. range]	Derivation (main feat.)	Current system	Reference
Low	Dst	1 hr	Global	4	Average of H	RC	Sugiura (1964)
Mid	SYM-H/D	1 min	Global	6	Average of H/D	Symmetric RC in N-S/E-W	Iyemori (1990), Iyemori et al. (2010)
	ASY-H/D	1 min	Global	6	Max − Min {H}/{D}	Asymmetric RC in N-S/E-W	Iyemori et al. (2010)
	SMR00	1 min	21–3 MLT	All available [−50°, +50°]	Average of N	PRC (midnight)	Newell and Gjerloev (2012)
	SMR06	1 min	3–9 MLT	All available [−50°, +50°]	Average of N	PRC (dawn)	Newell and Gjerloev (2012)
	SMR12	1 min	9–15 MLT	All available [−50°, +50°]	Average of N	PRC (noon)	Newell and Gjerloev (2012)
	SMR18	1 min	15–21 MLT	All available [−50°, +50°]	Average of N	PRC (dusk)	Newell and Gjerloev (2012)
	SMR	1 min	Global		Average of SMRhh	RC	Newell and Gjerloev (2012)
	MPB	1 min	18–6 MLT	All available (20°, 50°)	Average of X, H	FACs	McPherron and Chu (2017)
High	AU/AL	1 min	Global	12 [60°, 70°]	Max/Min {H}	East/West auroral electrojet	Davis and Sugiura (1966)
	AE	1 min	Global		AU-AL	Global electrojet	Davis and Sugiura (1966)
	SMU/SML	1 min	Global	∼120–140 [40°, 80°]	Max/Min {N}	East/West auroral electrojet	Newell and Gjerloev (2011a, 2011b)
	SME	1 min	Global		SMU-SML	Global electrojet	Newell and Gjerloev (2011a, 2011b)

Note. It includes: the latitude (low-, mid-, and high-latitude) zone, the longitudinal range covered (indicating the sector or global), the temporal resolution, the number of stations (or alternatively the latitudinal range covered by the stations) that are used to derive them, the main feature of their derivation, as well as the main representative current system (ring current (RC), partial ring current (PRC), field-aligned currents (FACs)). Last column gives references for each index.

of the equatorial RC, ASY-H contributes similarly to the asymmetric part (PRC) (Iyemori et al., 1992). On the other hand, the D component of the geomagnetic field is considered a good indicator of the contribution of FACs (Iyemori, 1990; Menvielle et al., 2010, pp. 220–221). Therefore, SYM-D and ASY-D indices are able to monitor the effect of the variation of FACs and ionospheric currents at midlatitudes. The effect of the PRC is expected to be smaller in the D component than in the H component (Fukushima & Kamide, 1973) and because the symmetric part of the D component is small in general, the value of ASY-D approximately indicates the disturbance due to FACs itself (Iyemori, 1990). Moreover, the effect of ionospheric currents are expected to be smaller than that of the FACs (Harel et al., 1981; Sun et al., 1984).

Four double H-spike events appear in Figure 4 as examples of selected case studies from those included in Table 2. They occurred during the geomagnetic storms on 11 April 2001, 8 April 2001, 25 September 1998, and 27 March 2017. In each plot, the top panel shows the auroral SML (blue) and SMU (red) indices, and the following panels show several mid-latitude indices; from up to down, the sector SMR12 (orange) and SMR00 (blue) indices along with the SMR (black) index, which is the average of the four sector SMR indices (see Table 3), the SYM (blue) and ASY (red) indices for the H component, and finally the SYM (blue) and ASY (red) indices for the D component. A box delineated by gray solid lines marks the time interval where the remarkable double H-spike occurs, as seen in the sector SMR12 and SMR00 indices. Likewise, each plot corresponds to a double-H spike occurring at a different stage of development of the geomagnetic storm (early, middle, late main phase and recovery phase), which is indicated in the upper right corner. Black dashed vertical lines mark the SSCs in the period shown. The SSCs are given by the International service on rapid magnetic variations at Ebro Observatory in Spain (https://www.obsebre.es/en/rapid). The intensity of the double H-spike, as defined by the peak value of Equation 1, is also indicated in each plot.

An additional case study appears in Figure 5, with the same format as that of Figure 4. It corresponds to a double H-spike event that occurred during non-storm time, that is, occurred after a prolonged low-activity (PLA) keeping the conditions during at least 10 hr before. The average Dst value during those 10 hr is about −10 nT. Only two other PLA events were detected in the period analyzed from 1998 to 2020: those that occurred on 17 March 2003 and 13 November 2003 (see Table 1).

The graphs of the remaining events selected as case studies and listed in Table 2 have been included in Appendix A.

Taking a look at the plots of the 12 double H-spike events selected as case studies (Figures 4, 5, and A1–A7) reveals that all double H-spike events are featured by a considerably active ground magnetic response at all latitude zones (pay attention to the time intervals marked by the boxes delineated by vertical gray lines). Effectively,

1. The double H-spikes, identified by the sector SMR00 and SMR12 indices, combine with significant auroral activity as seen by enhancements in the time series of SML and SMU indices occurring at the same time as the double H-spikes.
2. Enhanced geomagnetic disturbances are well distinguished in ASY-H and ASY-D indices during the double H-spike. However, SYM-H and SYM-D do not appreciably change during that time interval, regardless of the stage of the storm in which it develops.

Table 4 summarizes the peak values reached by different indices during the time interval corresponding to the double H-spike event. In this case the events have been sorted by decreasing SML_{peak} strength. It is notable that 8 out of 12 case studies (67%) occurred during a very intense auroral activation ($SML_{peak} \leq -2{,}000$ nT), which also correspond to the most intense values of $Range_{peak}$. For the total sample of events (see Table 1), the percentage we obtain is 62% (28 out of 45 events). In any case, the percentage changes to 100% when $SML_{peak} \leq -1{,}200$ nT. It can also be noticed that SYM-D is about 50 nT or less in 10 out of 12 events. Therefore, according to Iyemori (1990), ASY-D represents the major part of the disturbance.

Next, we outline what is known of correlations/associations between the high and mid latitude indices. Past works already found correlations between the various geomagnetic indices used to quantify the level of global magnetic activity observed at different latitude ranges, with the AE and SYM/ASY indices as those commonly used for the high and mid-latitude ranges, respectively. The SML and SMU indices used in this paper, instead of AE indices, are equivalent to the AL and AU indices, respectively (Ohtani & Gjerloev, 2020) (see also Table 3). From previous studies of those indices, we find that the index AE not only correlates well with the ASY-H index (e.g., Clauer & McPherron, 1980; Crooker, 1972) but also with the ASY-D index. Menvielle et al. (2010) argued that the good correlation with ASY-D is probably due to FACs. As part of the magnetosphere-ionosphere coupling system,

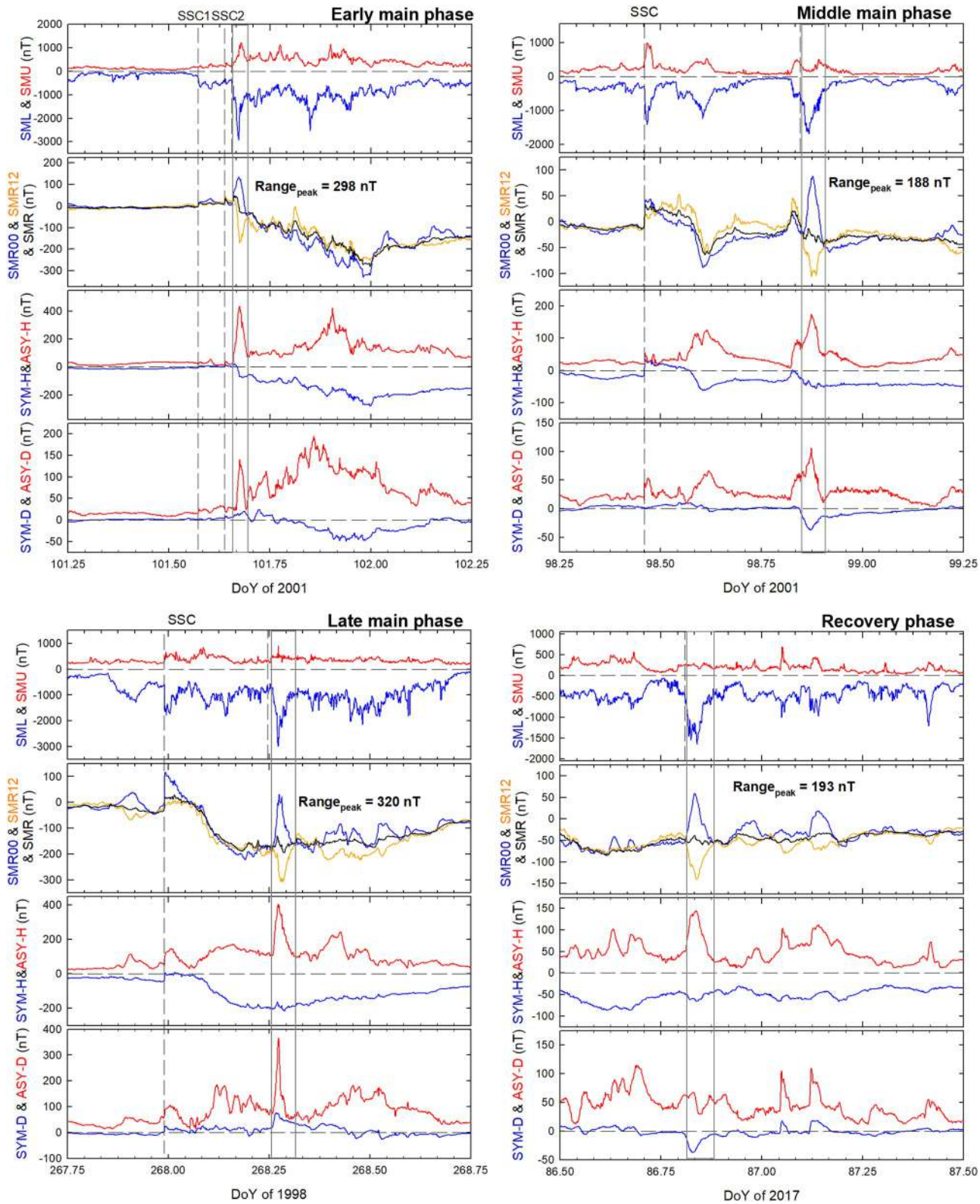

Figure 4. Four events featuring double H-spikes taking place during different stages of development of the geomagnetic storms, as appears on the upper right corner of each plot: early, middle or late main phases or recovery phase. Vertical dashed lines mark the storm sudden commencements, and boxes delineated by solid gray lines mark the intervals of the double H-spikes.

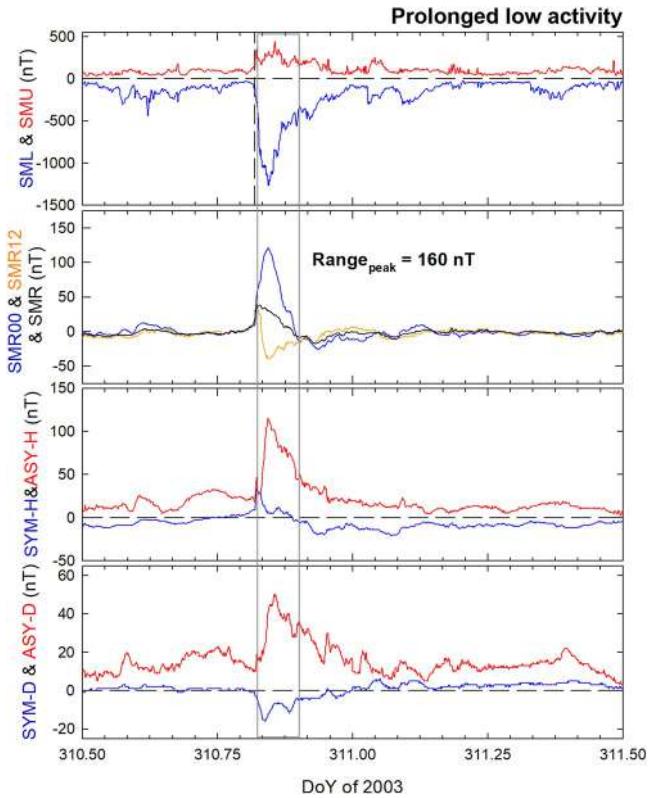

Figure 5. Double H-spike event featuring a prolonged low-activity (Prolonged Low Activity) period. The format is the same as Figure 4.

Table 4
Peak Values Reached by Some Global Magnetic Indices During the Double H-Spike Events Listed in Table 2

Double H-spike event (yyyy/mm/dd)	Range$_{peak}$ (nT)	SML$_{peak}$ (nT)	SYM-D$_{peak}$ (nT)	ASY-H$_{peak}$ (nT)	ASY-D$_{peak}$ (nT)
2005/08/24	385	−4,141	−20	236	303
2005/01/21	235	−4,035	−26	397	117
2003/10/29	682	−3,637	104	719	429
1998/09/25	320	−2,981	76	404	366
2001/04/11	298	−2,921	20	439	140
2005/01/07	317	−2,450	−51	284	221
2010/04/05	171	−2,307	−5	153	205
2000/09/17	296	−2,025	−51	188	162
2003/03/17	157	−1,743	−21	131	90
2001/04/08	188	−1,671	−37	175	106
2017/03/27	193	−1,649	−37	140	67
2003/11/06	160	−1,264	−16	115	50

Note. The list has been sorted by decreasing SML$_{peak}$ strength. Column 3 gives the maximum value reached by SML when the *Range* index reaches the value given by Range$_{peak}$.

connecting with auroral electrojets in the ionosphere, FACs generate ground magnetic disturbances whose effects can be observed even at midlatitudes. However, they also pointed out that the smoother variation of ASY indices respect to the variation of AE indices causes ASY to have less sensibility to minor substorm activities.

The global analysis of the 12 case studies reveals the simultaneity of enhancements in ASY and auroral indices, indicating that double H-spikes are a global phenomenon (extended both in latitude and longitude). This outcome, together with the results obtained in previous works in literature (some of them mentioned above) can be gathered to form a line of argument. Indeed, it is known that the auroral SML and SMU indices represent the magnetic effect of the westward and eastward electrojets and these are closely related to FACs as currents that feed them in the ionosphere. Although the magnetic effects from FACs and the ionosphere are superposed, the former are slightly greater than the latter at midlatitudes (Harel et al., 1981; Kikuchi et al., 2001). As ASY-D can be assumed to represent the disturbance itself, ASY-D would be reflecting mostly the effects of FACs that connect poleward the station. Therefore, it allows us to derive a first result in agreement to Fukushima and Kamide (1973), Nakano and Iyemori (2005), Shi et al. (2006), and Menvielle et al. (2010): that FAC effects would be dominating the asymmetric ground disturbance fields during the midlatitude double H-spikes. More evidence supporting this first result will be given in next subsections.

In Figure 6 we show three scatter plots of the peak values for the *Range* index (upper), ASY-H (center), and ASY-D (bottom) indices versus the minimum value reached by SML from the event onset to the time of its Range$_{peak}$ (SML$_{min}$). This parameter better guarantees the possible "cause-effect" relationship since it prevents SML$_{peak}$ from being reached at some time after Range$_{peak}$ (see, e.g., the upper panel in Figure A1). The plots include all 45 double H-spike events of Table 1. The correlation coefficients for Range$_{peak}$ is 0.53, for ASY-H$_{peak}$ is 0.62 and for ASY-D$_{peak}$ is 0.57. Correlation coefficient values around 0.6 are not very high, supporting only a weak relationship between the indices analyzed. This weakness may be associated with the complexity and variety of current sources that contribute to the disturbances at the location of a specific observatory.

Additionally, 10 out of 12 events present values ASY-D$_{peak}$ < ASY-H$_{peak}$ (columns 5 and 6 in Table 2). Similar outcome was observed in the whole sample of events (Table 1): 40 out of 45 events present values ASY-D$_{peak}$ < ASY-H$_{peak}$. One of the reasons for this result might be the magnification of the H component by the effect of FACs as it was already pointed out by Menvielle et al. (2010) and it would indicate that the latitude (λ) correction for each observatory disturbance by cos(λ), used in the procedure to obtain midlatitude global geomagnetic indices, might not be enough to minimize the effect.

4. Double H-Spikes and the Substorm Phenomenon

After being aware that all case studies occurred under significant auroral activity levels, and being pointed out FACs as the cause for the effects observed at midlatitudes, we explore in this section the relationship between the double H-spikes and the physical phenomenon of substorm, which constitutes a fundamental mechanism of deposition of energy into the magnetosphere, ionosphere and thermosphere (Akasofu & Chapman, 1964; Liou et al., 2001; Østgaard et al., 2005; Rostoker et al., 1980).

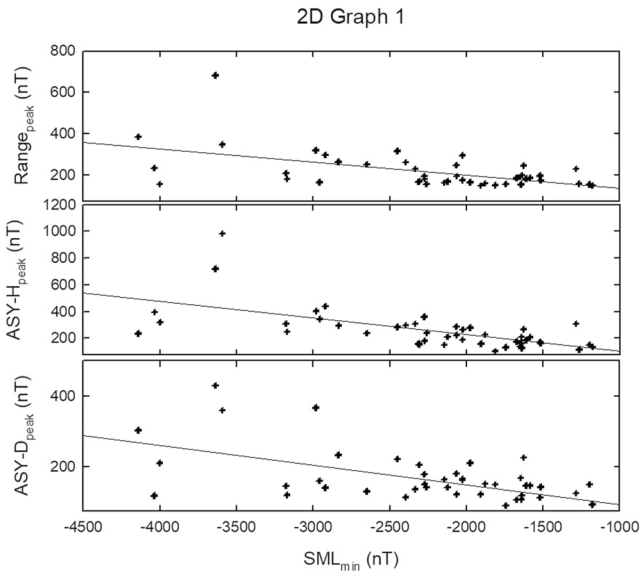

Figure 6. Relations between global indices during double H-spikes of ≥150 nT intensity (all events listed in Table 1 are included). Panels show the relation between Range$_{peak}$ (upper), ASY-H$_{peak}$ (center) and ASY-D$_{peak}$ (bottom) and the minimum value of the SML index, SML$_{min}$ (see text). The solid line in each plot represents the line of the linear fit.

4.1. Correspondence With Substorm Onsets

For that purpose we examined two public lists of substorms that are available on the SuperMAG website (https://supermag.jhuapl.edu/substorms/): Newell and Gjerloev (2011a, 2011b) *substorm list* and Forsyth et al. (2015) *substorm list*. These lists are obtained from the SML index and the procedures used in the derivation are described in the papers by Newell and Gjerloev (2011a, 2011b) and Forsyth et al. (2015). Likewise, we also used the McPherronMPB onset list, which is obtained from the MPB index as indicator of substorm onset at midlatitudes (McPherron & Chu, 2018). These authors have made the onset list available in the Supporting Information on (Data Set S4) of their paper.

Table 5 shows the result of our identification work. The onset time of the substorm is also marked by a vertical black dashed line in the SML and SMU panel (upper panel) of Figures 4, 5, and A1–A7. The events in Table 5 are sorted by increasing intensity according to Range$_{peak}$. The onset time of the double H-spike, as determined by *Range*(*t*), is given in column 3 and the duration of the event in column 4. The following three columns provide substorm onset time, MLT and magnetic latitude given by Newell and Gjerloev (2011a, 2011b) *substorm list* on the SuperMAG website (Newell & Gjerloev, 2011a, 2011b); column 8 gives the delay (in minutes) from the substorm onset (column 5) and the double H-spike onset time (column 3). Like columns 5–7, columns 9–11 provide substorm onset time, MLT and magnetic latitude given by Forsyth et al. (2015) *substorm list* on the SuperMAG website (Forsyth et al., 2015). The MPB pulse onset time is given in column 12.

From the global evaluation of the results summarized in Table 5, we can highlight that there is a full correspondence between the double H-spike and the substorm as each onset of the double H-spike development is associated to an onset of the substorm expansion phase. Most of the double H-spike onsets occur a few minutes later than the substorm onsets. This delay (see column 8) may arise because of the procedure followed in order to set the onset

Table 5
Relation Between the Double H-Spikes and Substorm Phenomenon Through SuperMAG Substorm Lists and Midlatitude Positive Bay Pulse List

H-spike event (yyyy/mm/dd)	Range$_{peak}$ (nT)	t_i (hh:mm)	Duration (min)	Onset[a] (hh:mm)	MLT (h)	MLAT (°)	Delay (min)	Onset[b] (hh:mm)	MLT (h)	MLAT (°)	Onset[c] (hh:mm)
2003/03/17	157	20:54	116	20:54	22.86	66.63	0	20:53	5.16	66.12	20:52
2003/11/06	160	19:44	118	19:40	22.09	67.37	4	19:36	22.03	66.21	19:38
2010/04/05	171	08:46	99	08:38	0.4	64.28	8	–	–	–	09:00
2001/04/08	188	20:16	79	20:16	5.79	65.13	8	20:11	5.69	65.13	20:18
2017/03/27	193	19:27	100	19:25	0.42	61.94	4	–	–	–	–
2005/01/21	235	17:26	80	17:24	6.02	68.8	2	17:00	1.24	66.17	17:24
2000/09/17	296	21:13	52	20:59	6.55	65.13	14	–	–	–	20:53
2001/04/11	298	15:49	52	15:43	4.21	65.24	6	15:39	6.55	69.48	15:43
2005/01/07	317	22:29	98	22:20	6.34	66.17	9	22:21	6.34	66.16	22:25
1998/09/25	320	06:09	83	05:54	21.65	62.14	15	06:05	6.88	57.9	06:11
2005/08/24	385	09:32	102	09:23	2.76	63.88	9	09:24	2.76	63.88	09:38
2003/10/29	682	06:12	87	05:59	23.76	68.75	13	05:59	23.75	68.75	06:42

Note. Columns 2–4 give the intensity, the onset time and duration of the double H-spike event, respectively. Two groups of three columns (5–7 and 9–11) provide substorm onset time, magnetic local time and magnetic latitude given by the two SuperMAG substorm lists. Column 8 gives the delay in columns 3 and 5. Last column gives the onset time of MPB pulses.

[a]Onset from Newell and Gjerloev (2011a, 2011b) list. [b]Onset from Forsyth et al. (2015) list. [c]Onset from McPMPB list.

time of the double H-spike by our simultaneous visual inspection of the SMR12 and SMR00 indices, or even because the indices are an average of the disturbances given by all the available stations in a 6-hr MLT sector.

In the systematic analysis of this work we have not considered the Ohtani and Gjerloev (2020) *isolated substorm list* (Ohtani & Gjerloev, 2020), which is also available on the SuperMAG website noted previously, but we checked it and we confirmed that it also includes one of the isolated substorm whose expansion phase started on 6 November 2003 at 19:38 UT, 6 min before the onset time of the double H-spike occurred on that date at 19:44 UT (see event #7 in Table 2). This event will be discussed later in Section 5.

The onset MLT values in Table 5 cover a wide longitudinal range on the nightside. It is also noteworthy that in 4 events out of 12 case studies (Table 5) the MLT sector of the substorm onset is the premidnight sector (>22 MLT); however, in the other 5 the onset is located into the dawn sector (~4–7 MLT).

4.2. Association With Supersubstorms

Regarding the severity of the substorms associated with the double H-spikes, the first five events (42%) in Table 4 correspond to extremely intense substorms, or supersubstorms (SSS) as labeled by Tsurutani et al. (2015) when SML $\leq -2{,}500$ nT. Comparing the information in Table 4 (sorted by SML) and in Table 2 (sorted by date) regarding these five case studies we find out that two occurred during intense storms, two in extreme storms and one in moderate storm. Moreover, the first two events listed in Table 4 (SML about −4,000 nT), that is, the most severe SSS, occurred during an intense storm and a moderate storm, that is, not during an extreme storm as might be expected considering the extreme auroral activity.

Next we discuss the association of double H-spikes with supersubstorms as identified by Hajra et al. (2016). They reported a statistical study on a sample of 74 SSSs occurring in the period 1981–2012. They found that in that period, 49% were associated with extreme geomagnetic storms, 46% with intense storms and 1% with moderate storms. The distribution of the number of SSS events per year and their SSS solar cycle dependence is shown by Hajra et al. (2016) in their Figure 3. Considering the whole list of double H-spike events, and not limiting the analysis to the case studies, 14 out of the 45 double H-spike events (Table 1) are associated with SSS: 57% during extreme, 36% during intense and 1% during moderate storms. These percentages of SSS follow the same trend, with the category of the storm according to its intensity, found out by Hajra et al. (2016) in the period studied (1981–2012). Moreover, in the period 1998–2012, the common interval between both studies, the distribution of the number of double H-spike events per year (Figure 2, panel (a)) is fully equivalent to their distribution of the number of SSS events per year in that period (see Figure 3 in Hajra et al. (2016)). Furthermore, comparing the number of double H-spike events and the number of SSS events per year, the maximum difference, if any, occur only by two double H-spike events more than SSS (in years 2003 and 2006). As a consequence, we found the same solar cycle dependence for double H-spike events as Hajra et al. (2016) with SSS. The highest frequency in the descending phase and minimum frequency at solar minimum was also found by McPherron and Chu (2018) by studying the occurrence rate of midlatitude positive bay onsets (McPMPB) in the period 1982–2012. In addition, given the close relationship found out between double H-spikes and the substorm phenomenon, we note that the seasonal non-dependence suggested from panel (b) in Figure 2 (see Section 2.2), is in agreement with other studies carried out with substorms which also did not show any clear dependence on season (Borovsky & Yakymenko, 2017; Tanskanen et al., 2011).

Hajra et al. (2016) also carried out the superposed epoch analysis of the solar wind parameters (plasma and magnetic field) to identify the interplanetary structures causing so large values of SML_{peak}. From the superposed parameters, SSS events were related to enhanced density and pressure, intense southward IMF Bz (at least 1.5 hr before the average superposed SML_{peak} value), and IMF directional change. The close relationship found between double H-spikes and SSS events point out identical triggers for both events. Nevertheless, this is out of the scope of this paper and a more detailed study of the triggers is foreseen in a future paper.

4.3. Ground Magnetic Disturbances as Remote Effects of FACs

Ohtani et al. (2021) examined ground magnetic disturbances in the nightside subauroral zone during two isolated substorms. By comparing ground magnetic disturbances and magnetic field measurements made by the SWARM spacecraft above the ionosphere, Ohtani et al. (2021) concluded that substorm-related ground geomagnetic

Table 6
Peak Values Reached by the Global Magnetic Indices During the Three Prolonged Low Activity Events

PLA event (yyyy/mm/dd)	$< Dst >_{10h}$ (nT)	$Range_{peak}$ (nT)	SML_{peak} (nT)	$SYM\text{-}D_{peak}$ (nT)	$ASY\text{-}H_{peak}$ (nT)	$ASY\text{-}D_{peak}$ (nT)
2003/03/17	−40	157	−1,743	−21	131	90
2003/11/06	−10	160	−1,264	−16	115	50
2003/11/13	−25	156	−1,644	−37	140	67

disturbances were the remote effects of the SCW. Moreover, the correlated magnetic disturbances extend to the midday sector. Indeed, with a set of 6,700 isolated substorm onsets identified with SML in the period 1995–2018, they statistically examined the correlation between mid-latitude and high-latitude geomagnetic indices (specifically between SMR12 and SMU12, between SMR12 and SML12, and between SMR12 and SMLN). From the magnitude of the correlated variations, they inferred that midday magnetic disturbances at both midlatitudes and high latitudes are remote effects of the SCW, which strongly suggests that even in the midday sector the remote effect of the SCW is more important than the effect of the dayside magnetosphere-ionosphere current system, that is, of the effects of the dayside FACs. Therefore, the contribution of midlatitude ionospheric currents on the ground magnetic disturbances during substorms is relatively small on both the nightside and the dayside. The relationship that we have found between double H-spike events, detected at midlatitudes with the SMR12 and SMR00 sector indices, and the substorm expansion events, detected at auroral latitudes with the SML index, fully agrees with Ohtani et al. (2021), which allows us to conclude that FACs effects at midlatitudes are predominant during double H-spikes.

On the other hand, we are aware that the RC is an important contributor to SMRhh during storms and we must be cautious with the generalization of the results obtained by Ohtani et al. (2021) from a study with isolated substorms. Nevertheless, there are some clues which allow us to strongly suggest a scenario as follows: as the substorm expansion starts, a SCW system will form mainly on the nightside, which can extend well in longitude, and the region-1 system will change globally in correlation with the nightside westward electrojet. The remote effects of this SCW system will be simultaneously seen on both the nightside and dayside ground magnetic disturbances. The double H-spike detected during that substorm will be the remote effect of the SCW but observed at midlatitude stations. On the nightside the magnetic disturbance is observed as a positive H-spike as corresponding to stations located within the SCW system and on the dayside the magnetic disturbance is observed as a negative H-spike as corresponding to stations located out of the SCW system (as expected from the Biot-Savart law). Therefore, the negative spike observed on the dayside, which one might expect not to be associated with a nightside phenomenon, is the result of the remote effect of the SCW. On the other hand, this suggestion is supported by the observed simultaneity in both spikes, which indicates as associated to the same phenomenon. The day-night asymmetry is probably associated with the formation of the SCW system (Ohtani et al., 2021).

5. Double H-Spike Events During Non-Storm Time (Prolonged Low Activity Events)

Only three double H-spike events were identified with the SMR00 and SMR12 indices as occurring during non-storm time. Furthermore, each event started after at least 10 hr of low activity ($Dst \geq -50$ nT), this is the reason why we named PLA. Two of these events were selected as case studies (see Table 2). The third PLA event took place on 13 November 2003 (see Table 1). The PLA event detected on 6 November 2003 (Figure 5) was mentioned in Section 4 as an event associated with an isolated substorm of the Ohtani and Gjerloev (2020) *isolated substorm list.*

Now we analyze in more detail these events. In Table 6, we summarize the peak values reached by different global indices during the time interval corresponding to the PLA event. Their maximum intensity is 160 nT, close to the 150 nT threshold selected in our study. On the other hand, the SML peak values are $\leq -1{,}200$ nT.

These events, as simple elements of the complete sample of double H-spikes events, give support to the outcomes from Sections 3 and 4. Indeed, the peak values of SYM-D in the interval of interest are low and ASY-H > ASY-D (see columns 6 and 7), but SYM-H (Dst) is low, which indicates that the contribution of the equatorial RC is irrelevant. However, an asymmetric response in ground magnetic disturbances is detected by

midlatitudes indices, simultaneously with the occurrence of substorm expansion. Therefore, one more time everything points to the FAC effects at midlatitudes as causing the ASY-H enhancements during double H-spike events.

6. Double H-Spikes During Storm Time

Most of the double H-spike events listed in Table 1 occurred during geomagnetic storms. Indeed many of them were intense or even extreme storms and, as a consequence, a vast number of papers studied these storm events. In a few cases the authors made a detailed analysis of the storm interval that corresponds to that of the double H-spike. Thus, in this Section we will take advantage of their results to double check our previous outcomes on double H-spikes regarding their interplanetary triggers, their responsible current system or even their wide coverage. For this purpose we have made a literature review of storm or substorm events that occurred throughout the days of column 1 in Table 1 just focusing on the results concerning the interval of interest. Those events with some previous results are described below.

6.1. 25 September 1998

The double H-spike detected during the magnetic storm on 24–25 September 1998 is the event #1 of the case studies (see Table 2), with onset at 6:09 UT on 25 September and the peak value reached at 6:36 UT. It takes place during the late main phase of the storm a few minutes after a supersubstorm (SML $\sim -2{,}900$ nT, see Figure 4). Among the number of papers studying this intense storm ($Dst_{peak} = -202$ nT at 8 UT on 25 September), Lukianova (2003) focused on the response to a strong solar wind pressure pulse (up to 25 nPa) observed at 6:00–6:50 UT on 25 September during a period of southward IMF. Note that the time interval studied corresponds well with that of the double H-spike. Lukianova (2003) noted that the signature seen in the SYM-H index during the time interval of the response to the pulse (a wave-like perturbation, first positive and then negative) is different from a simple positive bay that usually indicates the increased Chapman-Ferraro (CF) current due to the pulse passage. Indeed, low and mid-latitude ground observations show a positive bay from the stations located in the night local time sector, whereas clearly show a negative bay from the stations located on the dayside (see Figure 2 of Lukianova (2003)), being the strongest response near the local noon. She concluded that the negative bay observed at low and midlatitudes on the dayside would be the effect of strengthening of R1 FACs in direct response to the pressure pulse. Her conclusion agrees with the results obtained by Shi et al. (2008) by modeling the magnetospheric current response to solar wind dynamic pressure enhancement during the interval of interest. Shi et al. (2008) concluded that the asymmetric low and mid-latitude H perturbations are primarily due to a net FAC system, which includes the R1 and R2 FACs and the closure FAC of the PRC. Within the context of this net FAC system, R1 and R2 have opposite contributions, with the R1 contribution always being larger than that of R2; therefore, this imbalance is primarily responsible for the negative (positive) H perturbations on the dayside (nightside).

6.2. 11 April 2001

Two supersubstorms, with a peak value of the SML index of −2,923 and −2,524 nT, respectively, and separated about 4 hr, occurred during the main phase of the magnetic storm on 11 April 2001, well ahead of the storm peak intensity (Hajra et al., 2016). A shock at 15:53 UT coincides with the time of the first SSS event onset, for which a southward turning of IMF Bz 39 min prior to the onset along with a pressure pulse from 9 to 24 nPa across the shock were pointed out as the interplanetary features for the SSS event (Hajra et al., 2016). For the second SSS event the onset also corresponds to a southward turning of the IMF Bz but solar wind parameters did not seem to have any associated pressure pulse, but high maintained values (Vsw ~ 744 km s^{-1}, Nsw ~ 23 cm^{-3}, and Psw ~ 24 nPa). It is interesting to note that, while a double H-spike was detected (case study event #4 in Table 2) with a large intensity ($Range_{peak} = 298$ nT) during the first SSS event, during the second one it was not detected (see Figure 4), despite the similar intensity of both supersubstorms. This result raises the question about the actual interplanetary conditions that trigger double H-spikes on the ground magnetic disturbances at midlatitudes, reinforcing the relevance of the pressure pulse against the large pressure values. This issue is out the scope of this paper and will be studied in the near future.

6.3. 29 May 2003

Shi et al. (2008) modeled the magnetospheric response at low- and mid-latitudes to solar wind dynamic pressure enhancements during different phases of geomagnetic storms. The onset of one of those pressure enhancements happened at ∼19 UT on 29 May 2003. Then, a large and abrupt increase of the ASY-H index was detected indicating strong ground asymmetric H perturbations at midlatitudes. A polar plot MLT-MLAT of all available stations at those latitudes shows a clear day-night pattern during the pressure enhancement: positive (negative) H perturbations on nightside (dayside) (see Figure 1b of Shi et al. (2008)). A double H-spike occurred on 29 May 2003 (Table 1) during the main phase of the intense storm ($Dst_{peak} = -144$ nT). The $Range_{peak} = 231.2$ nT was reached at 19:13 UT. Shi et al. (2008) modeled ground H perturbations in the interval 18–21 UT of this storm, thus including the interval of the double H-spike event. The model fits well the observed day-night asymmetry pattern and their results show the net FAC system from R1, R2, and PRC as responsible for this polarity, with the R1 FACs having the most significant contribution at all MLT sectors, being this stronger effect primarily responsible for the negative H perturbation at noon and the positive one at midnight.

6.4. 29 October 2003

Among the vast amount of papers devoted to different aspects of the Halloween storms our target is the ground magnetic response beginning at 6:12 UT on 29 October 2003, just after the SSC that occurred at 6:10 UT, and lasting about 90 min. This time interval corresponds to the double H-spike event #6 of the case studies (see Table 2), with $Range_{peak} = 682$ nT reached at 6:57 UT while a substorm expansion was taking place (SML ∼−3,660 nT). Note that this double H-spike has the highest $Range_{peak}$ intensity recorded in at least the last two solar cycles. Yamauchi et al. (2006) studied the unusually quick development of this supersubstorm during the first 10 min shortly after the SSC. Note that the strong decrease/increase in the SMR00 and SMR12 indices (see Figure A3) occurred after the initial 10 min. They showed that the large magnetic disturbance is the result of two independent activities which started simultaneously, one in the evening-midnight sector and the other in the morning sector, merging both of them during the substorm expansion at the high-latitude sector. Yamauchi et al. (2006) pointed out the ionospheric current as responsible for the large asymmetry observed in the mid-latitude ground disturbances, as it is reflected in both ASY-H and ASY-D indices, by arguing that the effect of the FAC and Pedersen currents are mostly canceled out. The most recent work we know about this storm is that of Ohtani (2022), which is devoted to identify the source current system of the very large H depression observed at midlatitude late morning stations during the 2003 Halloween storm. Contrary to Yamauchi et al. (2006), Ohtani concludes that the observed N depression was a remote effect (as expected from the Biot-Savart law) of a dayside R1-sense SCW formed in the auroral zone, where the process was global as it is well reflected by the enhancements in all sector SML indices. Furthermore, for the similarities in characteristics, Ohtani (2022) suggests that the 1,600 nT H depression recorded at Colaba (ABG) during the 1859 Carrington storm was also caused by this kind of current system. Similarities between both the Halloween and the Carrington storm were also found by Cid et al. (2015). FACs as a trace involved in that large negative spike observed at late morning stations during the large day-night asymmetry were suggested by Saiz et al. (2016, 2021).

6.5. 14–15 December 2006

On 14 December, during the middle of the main phase of an intense storm ($Dst_{peak} = -160$ nT), a double H-spike developed reaching $Range_{peak} = 247$ nT at 23:56 UT (see Table 1). The magnetic storm was analyzed by Ohtani et al. (2018). They investigated the formation and development of the large-scale dawnside wedge current system during intense geomagnetic storms paying attention to the westward *E* component deflections of the morningside midlatitude magnetic field. Specifically, on 15 December at 00:00 UT (only 4 min after reaching the double H-spike peak value), the *E* component measured at midlatitude Memambetsu (MMB) station is the fourth most intense in the rank of the 10 largest hourly westward deflections from 1987 to 2016 (see Table 1 of Ohtani et al. (2018)). From the evolution of global equivalent currents carried out around the time, it was suggested that a SCW, consisting of upward and downward FACs at its ends (actually unbalanced parts of the R1 and R2 currents) closing with a westward electrojet formed in the postmidnight sector and then intensified and extended eastward. This is consistent with the significant enhancements of the ASY indices starting around 23:30 UT (Ohtani et al., 2018) and the occurrence of a substorm (onset on 14 December at 23:37 UT, MLT = 5.39 hr,

MLAT = 65.1°, SML_{peak} = −2,150 nT). Thus, the large ground perturbations observed at morningside midlatitudes were interpreted as a remote signature of the downward FAC.

6.6. 24 August 2005

On 24 August at 10:05 UT and at 10:30 UT two large SML deflections but distinct from each other occurred consecutively. Those times were considered by Tsurutani et al. (2015) as the initiations of two SSS events being SML intensities about −4,000 nT, giving a duration of 18 and 26 min respectively. Both events, were shown as examples of substorms externally triggered by solar wind pressure pulses of magnitude about 25 nPa (see Figure 4 of Tsurutani et al. (2015)). The double H-spike detected on 24 August 2005 corresponds to the case study #10 in Table 2. As can be seen in Figure A6, the two large SML deflections are part of the interval of the substorm with onset at 9:23 UT (see Table 5). Note that at midlatitudes, the SMR12 and SMR00 indices do not distinguish the two activations as two different ones, so one only double H-spike was detected.

7. Potential Space Weather Effects During Double H-Spike Events

GICs are driven by the geoelectric field induced by fluctuations of Earth's magnetic field (Ngwira & Pulkkinen, 2019; Pulkkinen et al., 2005; Trichtchenko & Boteler, 2004; Viljanen, 1997; Viljanen et al., 1999) and can produce ground electrical anomalies in power transmission lines. As the physical cause of GICs are rapid time-varying magnetic fields (dB/dt), GICs will occur mainly during magnetic storms and substorms (Schillings et al., 2022; Tsurutani et al., 2015), and FACs can play an important role in producing large GICs at low latitudes during geomagnetic storms (Zhang et al., 2022). It is well known that substorms can occur as features outside storms (Iyemori & Rao, 1996; Trichtchenko & Boteler, 2004) but substorms are always an important feature within the timeline of any storm. In fact, most GIC events that arise during geomagnetic storms are strongly associated with substorm peaks. As an example, in the March 1989 geomagnetic storm, the largest storm of the last century (Dst_{peak} = −589 nT), large GICs that caused the blackout of the Hydro-Quebec power system, occurred during one substorm, and power system problems in Europe occurred during two much later substorms (Boteler, 2019).

To the extent that the double H-spike events correspond to high short-time magnetic field variations, we anticipate that during those periods likely large dB/dt will occur. Therefore, we foresee a potential risk of GIC occurrence at midlatitudes for double H-spikes. The purpose of this Section is to confirm if the expected association exists. We are aware that the process of assessing the response of the power grid to the geoelectric fields consists of two differentiated processes: (a) the process of estimating geoelectric fields, which are not affected by the electrical properties of the power grid but they are determined by the time derivative of the geomagnetic field and the properties of the Earth, and (b) the process of estimating the response of the power grid to those fields, which is determined by the electrical properties of the grid (network topology, electrical conductivity of the grid lines, transformers at substations and their connections to ground). The contribution of our study to the first of them is a first approach to evaluate the time derivative of the geomagnetic field.

We obtain time derivatives of the magnetic field at midlatitudes during the periods of the double H-spikes using the SMR12 and SMR00 indices. We assume the derivatives of both indices, dSMR12/dt and dSMR00/dt, as indicatives of the significance of the N component variations of the magnetic field on the dayside and the nightside, respectively. With regard to this, we must be cautious because the local derivative at one station can differ from the derivative of the index, which is the average of all available stations within the sector. Figure 7 shows the results of our analysis for all events listed in Table 2. A box delineated by vertical gray solid lines marks the interval of the double H-spike in each panel. Note that the vertical scale is different according to each event.

Viewing the panels of Figure 7, the general impression is that within all boxes delineated by vertical gray lines, which mark the double H-spike intervals, enhanced derivative values are distinguishable in both indices, that is, in the noon sector index and in the night sector index. And this is so, even during storm-time periods (see e.g., the panels of the events 7 January 2005, 17 September 2000, and 27 March 2017).

Schillings et al. (2022) investigated all storms from 1980 to 2020 and analyzed the $|dB/dt| \geq 500$ nT/min spikes in the N and E components using a worldwide coverage (high-latitude superMAG stations). Their results confirmed the existence of two zones with a higher occurrence frequency of dB/dt spikes, located in the pre-midnight sector

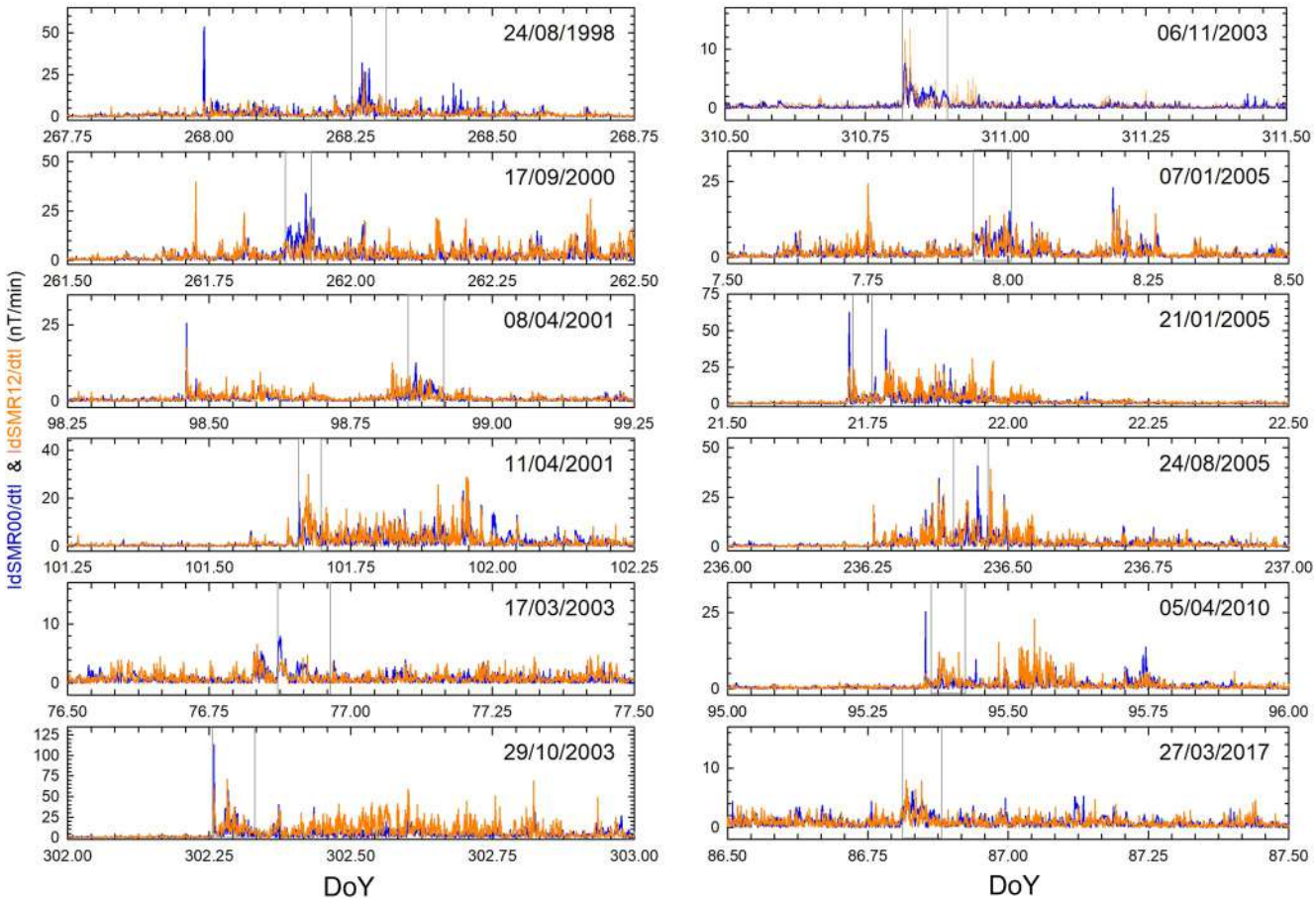

Figure 7. Time derivatives of the SMR00 (blue) and SMR12 (orange) indices. The events correspond to that listed in Table 2. A box delineated by gray marks the interval of the double H-spike.

and in the morning MLT sector. However, they also noted that there are some exceptions for which multiple MLT sectors were activated in the detection of *dB*/*dt* spikes, where the multiple activations resulted in sub-auroral magnetic latitudes rather than around the usual ∼65°. Likewise, they did not find any correlation between the *dB*/*dt* spike occurrence frequency and the Dst and AE indices during the duration of the storm. Table 1 of Schillings et al. (2022) provides a list of 27 storms with at least 10 recorded spikes. 10 out of those 27 events occurred during the dates listed in column 1 of Table 1 and they have at least 14 spikes.

Although to demonstrate that the double H-spike events have a potential space weather impact would be sufficient to demonstrate that they can generate the geomagnetic variations that we know will induce strong geoelectric fields, it is also worth noting some other observational results. Tsurutani and Hajra (2021) using measurements of the current intensity from a subauroral station in Finland, identified intense GIC events over a period from 1999 to 2019 (almost the same interval as the one covered by this study, 1998–2020). They found that the most intense GIC events were associated with intense substorms, and they presented a broad nightside distribution, from 20 MLT to 5 MLT, and a narrower one in the morning-noon sector extending from 9.5 MLT to 10.5 MLT. Note that those MLT sectors are well covered by the SMR00 and SMR12 indices (from 21 MLT to 3 MLT for SMR00 and from 9 MLT to 15 MLT for SMR12) used in our analysis. These results are, in our opinion, one more argument that supports that the double H-spikes that occur at midlatitudes, not only can induce significant GICs, but are also remote effects of FACs, and the negative H-spike detected on the dayside is part of the same current system. As an example, on 29 October 2003 (event #6 in Table 2) GICs > 50 A were measured and the station was located on the dayside at about 9 MLT.

In summary, all facts presented above converge toward the following outcome: double H-spike events pose a potential risk to damage the technology by generating GICs even at midlatitudes, in both dayside and nightside

sectors. The Halloween storm provides an example of this result: extensive damage to ESKOM power transformers located in a mid-latitude region occurred (Falayi et al., 2017; Gaunt & Coetzee, 2007; Thomson et al., 2010) and a power blackout in Malmö causing 50,000 customers to be without power for 20–50 min (Krafnät, Dnr/805, 2011). Excess heating in a transformer occurred on 30 October 2003 at 20:07 UT (Pulkkinen et al., 2005; Wik et al., 2009), just 11 min after the peak of a double H-spike of 349 nT intensity occurred at 19:56 UT on 30 October (Table 1). Recently, Nahayo et al. (2022) showed also GICs measured at Grassridge substation (33.7°S, 25.6°E), located at midlatitude in South Africa (near the Hermanus magnetic observatory), in the period 29–30 October (see Figure 2 of Nahayo et al. (2022)). As can be seen in that figure, significant GICs (~10 A) were recorded during the double H-spike with peak at 6:58 UT on 29 October and also during the double H-spike on 30 October mentioned above. On the other hand, Schillings et al. (2022) found $|dB/dt| \geq 500$ nT/min spikes between 50° and 90° MLAT as well as in almost all MLT ranges. They report that between 6:10 UT and 7:20 UT, 95 spikes were detected from the early evening sector 18.6 MLT to the late morning sector 9.2 MLT. That is the time interval of the first double H-spike on 29 October.

Finally, we note the potential space weather impact of the double H-spikes by showing that during those intervals, the sector SMR12 and SMR00 indices used to detect them, exhibit large geomagnetic variations, which are required to drive GICs. However, for the quantitative analysis would be needed both *dB*/*dt* and spectral content of the geomagnetic variations at the level of individual magnetometers. A topic for future work is to demonstrate whether ground signatures of the double H-spikes have strong variations at very low frequencies (a few millihertz) as those low frequencies can play a key role in generating strong geoelectric fields.

8. Summary and Conclusions

This paper reports, for the first time, a detailed statistical study on large magnetic disturbances, called double H-spikes, occurring from 1998 to 2020. This period comprises two solar cycles. From a systematic search, 45 events were identified using measurements from SuperMAG sector indices, specifically the sector SMR00 and SMR12 indices, setting the peak intensity threshold at SMR00–SMR12 $\geq$ 150 nT. Twelve events out of that set were selected as case studies. The main results and conclusions of the present study can be classified around four topics (summarized in the following subsections): the intensity and occurrence frequency of double H-spikes, their connection with high-latitude phenomena, the source of the longitudinal asymmetry observed at midlatitudes, and the potential space weather risk they pose.

8.1. Intensity and Occurrence Frequency

Our study has identified the following characteristics of the double H-spikes:

1. The double H-spike events have occurred during all phases of the solar cycle except during minima. The highest occurrence frequency was recorded in the Solar Cycle 23 descending phase. The frequency was considerably lower in the ascending phase and the lowest at solar minimum. Only a few events occurred during the descending phase of the Solar Cycle 24. The distribution does not present any clear seasonal dependence.
2. The double H-spikes intensity, as given by its Range_{peak}, is mostly within the 150–200 nT range, that is, close to the threshold of 150 nT. Nevertheless, a non-negligible quantity of events present greater intensity.
3. The phase of the storm does not characterize the events as they occur at any stage of their development: the main phase (early, middle or late), the recovery phase, or even during quiet or prolonged low geomagnetic activity. Only three events occurred in non-storm time, which suggests SML $\sim -1{,}200$ nT as threshold to detect $\text{Range}_{peak} \geq 150$ nT events.

8.2. Connection With High-Latitude Magnetic Activity

We have shown that each double H-spike observed at midlatitudes is simultaneous with a high-latitude magnetic activity period, as indicated by the auroral SML index, and with enhancements in ASY indices. Correlation coefficient between peak values of magnetic indices is ~0.6.

The physical magnetospheric phenomenon associated with double H-spike events is the substorm phenomenon. Therefore, the FACs, as currents participating in the M-I coupling system during the substorm expansion, would be playing a predominant role in the observed mid-latitude ground magnetic disturbances.

8.3. The Source of the Longitudinal Mid-Latitude Asymmetry

Numerous connections between our own analysis and the results from previous studies quoted along this paper lead to the conclusion that double H-spikes are a phenomenon of global nature, which extends to all longitudes, and the ground disturbances observed at midlatitudes are remote effects of FACs. Indeed the main source of this longitudinal asymmetry observed in the mid-latitude sector SMR indices (simultaneously a negative H-spike in the dayside sector and positive H-spike in the nightside sector) is the SCW, whose effects have an extended longitudinal range as expected from the Biot-Savart law. Therefore, enhancements in ASY indices during the double H-spike events would be indicating the latitudinal effect of FACs instead of the asymmetric contribution of the RC.

Some interplanetary parameters have been mentioned as causing the ground magnetic response object of study including pressure pulses, previous intervals of southward IMF Bz, IMF directional changes, etc. However, some unknowns remain to be answered. These are for example, the following: are there any other feature in the IP parameters that ensures the occurrence of a double H-spike of the observable intensity?; do the double H-spikes always arise from IP drivers (external drivers) or can they also result as part of the complex dynamics of the magnetosphere-ionosphere system? A detailed study of the parameters necessary for understanding the triggers and forecasting the double H-spikes is out of the scope of this paper, but will be carried out in a future paper.

8.4. Potential Space Weather Risk

Considering the study carried out connecting the double H-spikes with the time derivative of the sector SMR indices, and, also the space weather effects occurred during the double H-spike intervals that we have reported in several revisited storms, we highlight the potential risk these events can pose even for technology located at midlatitudes.

Appendix: Additional Double H-Spike Events A

The appendix includes the figures of double H-spike events listed in Table 2 not appearing in the main content of the paper (see Figures A1–A7).

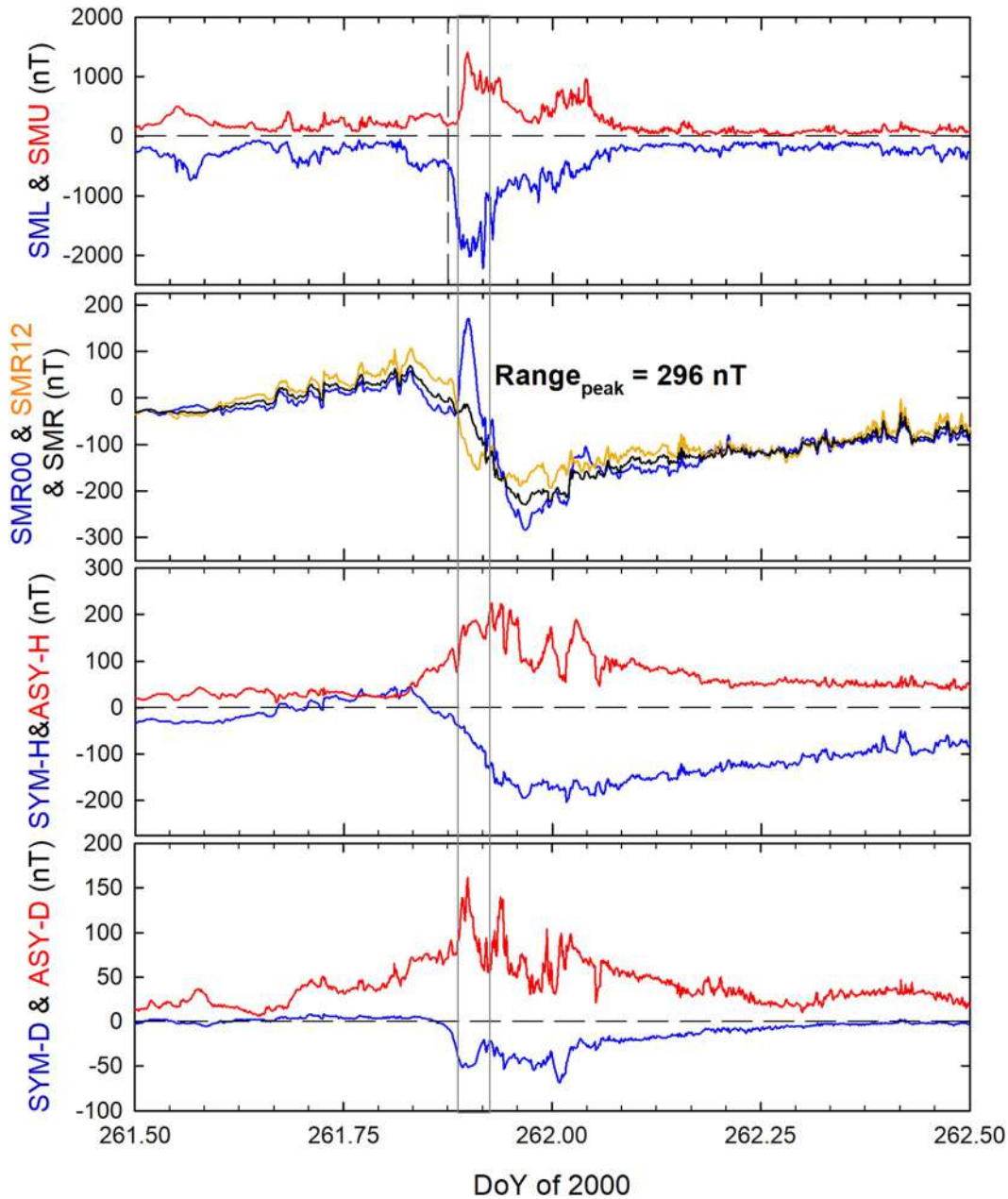

Figure A1. Double H-spike on 17 September 2000 (event #2 in Table 2). Auroral indices SML and SMU (top); sector indices SMR12 (orange) and SMR00 (blue) and SMR (black) (second panel); symmetric and asymmetric H-component indices SYM-H (blue) and ASY-H (red) (third panel); symmetric and asymmetric D-component indices SYM-D (blue) and ASY-D (red) (bottom). Horizontal dashed lines mark the zero value as reference. Pink shadow area shows the time interval of the double H-spike. The vertical dashed line on top panel marks the onset time of substorm as given by Newell and Gjerloev (2011a, 2011b) substorm list.

10.1029/2023SW003453

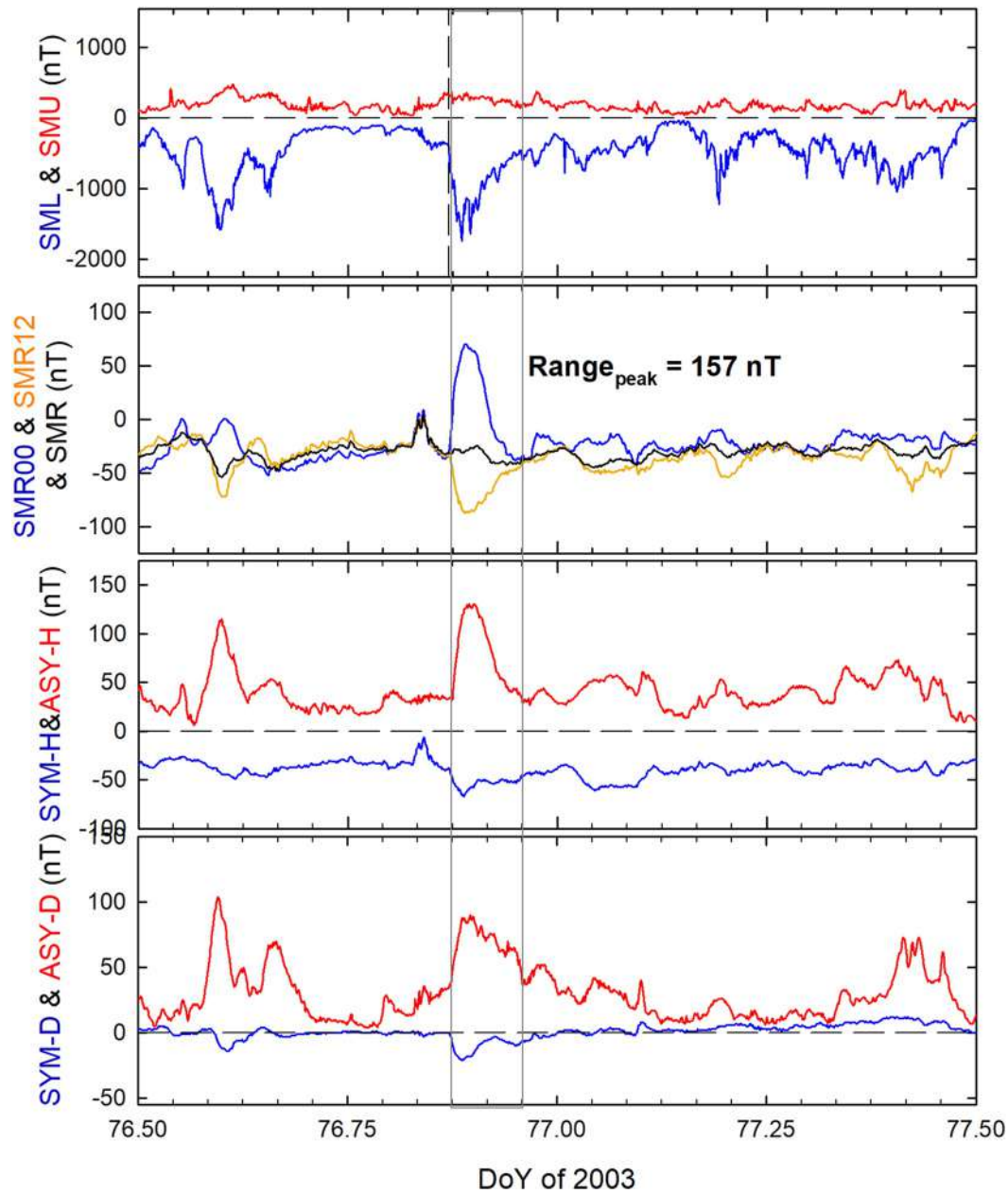

Figure A2. The event on 17 March 2003 (event #5 in Table 2). The format is the same as the one in the Figure A1.

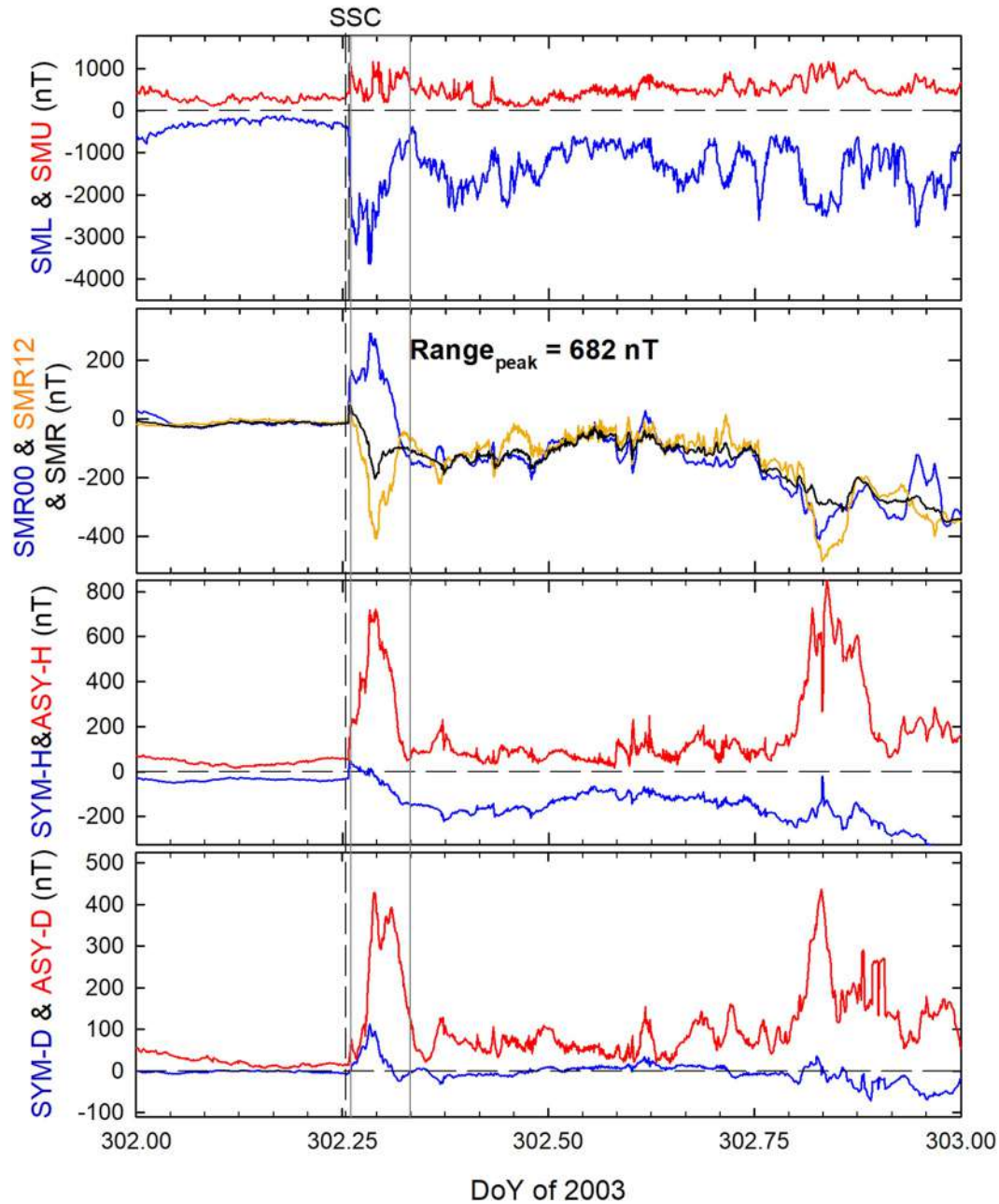

Figure A3. The event on 29 October 2003 (event #6 in Table 2). The format is the same as the one in the Figure A1.

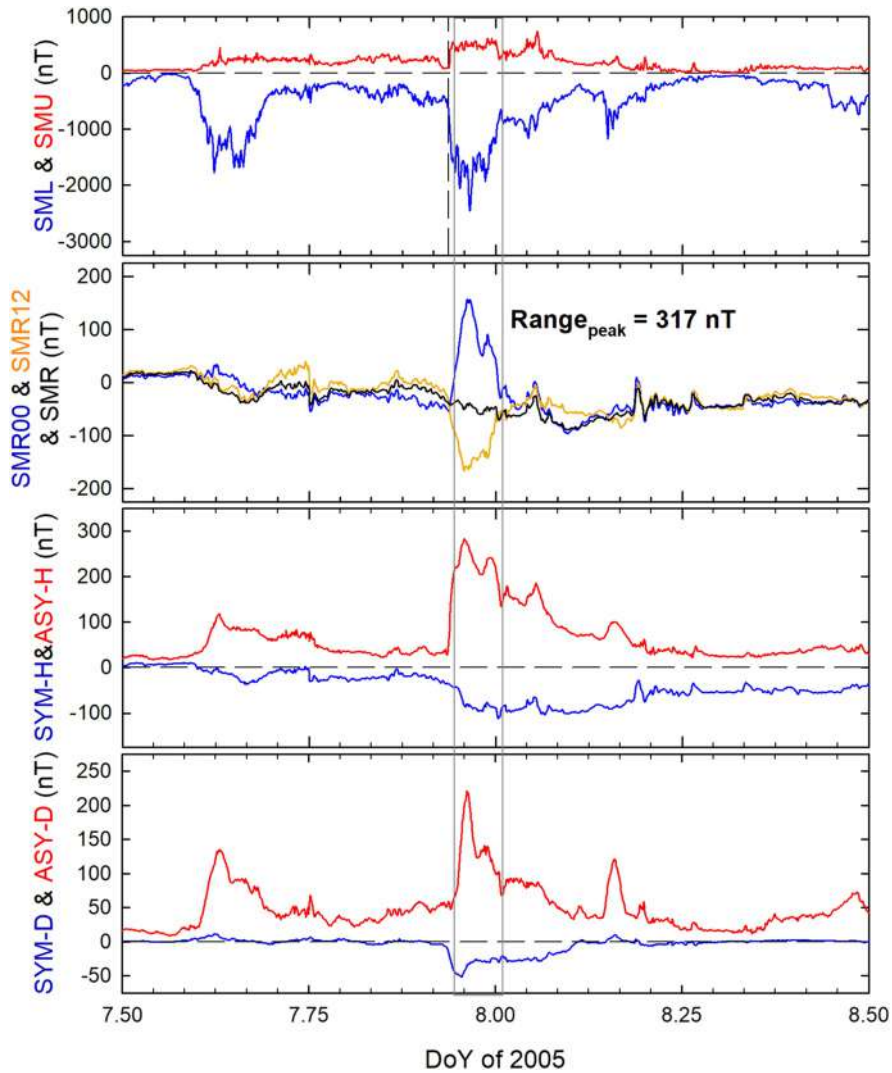

Figure A4. The event on 7 January 2005 (event #8 in Table 2). The format is the same as the one in the Figure A1.

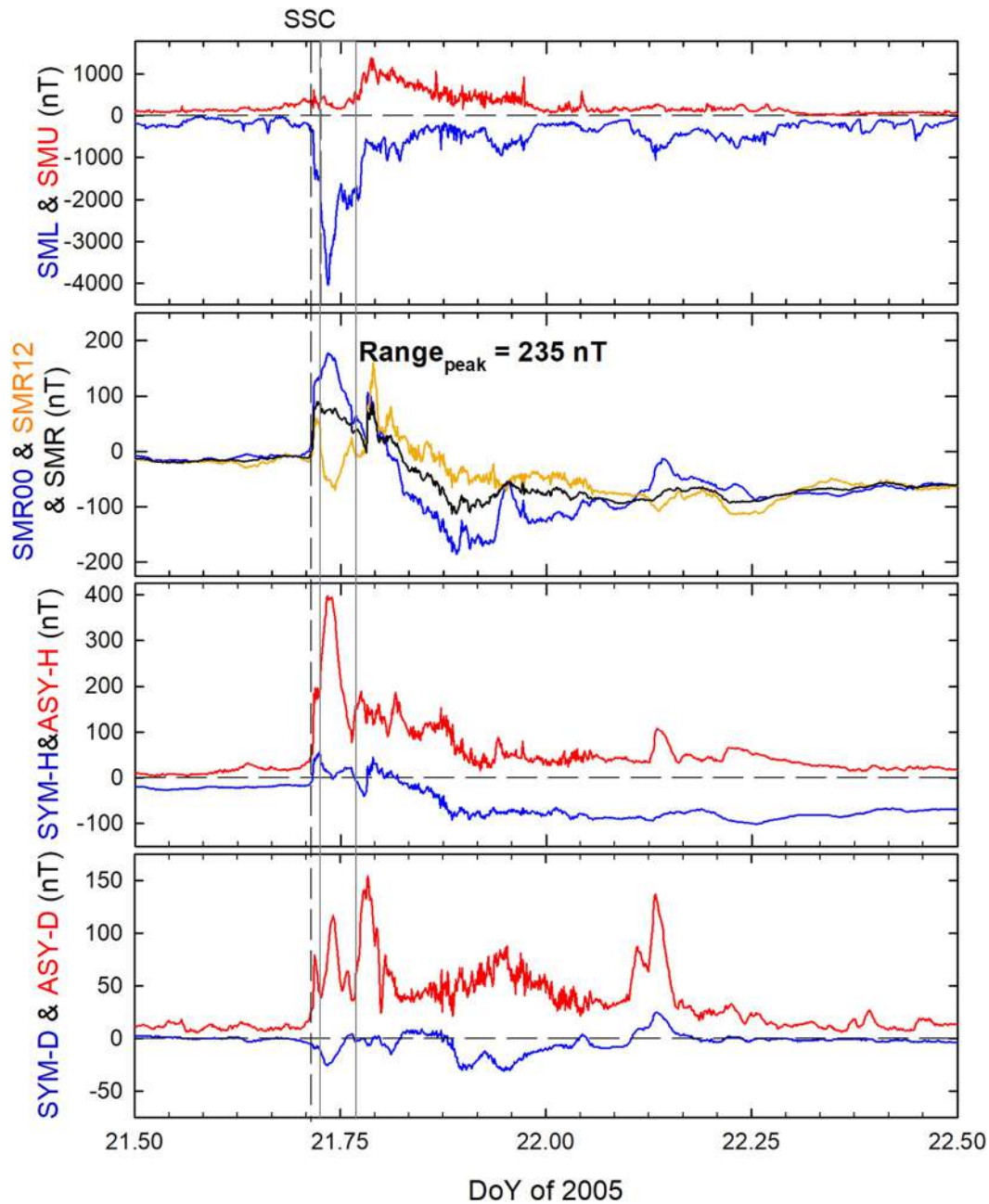

Figure A5. The event on 21 January 2005 (event #9 in Table 2). The format is the same as the one in the Figure A1.

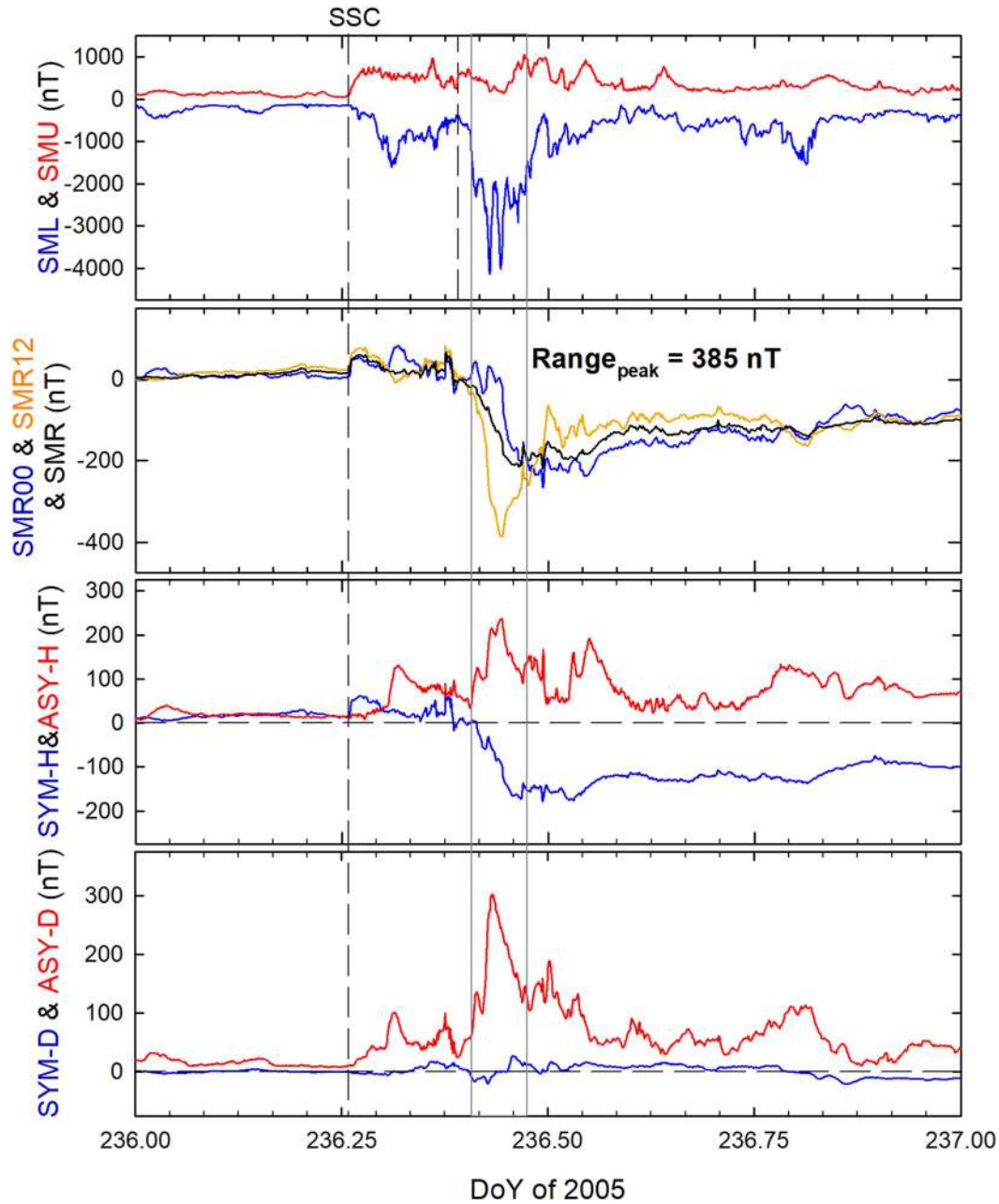

Figure A6. The event on 24 August 2005 (event #10 in Table 2). The format is the same as the one in the Figure A1.

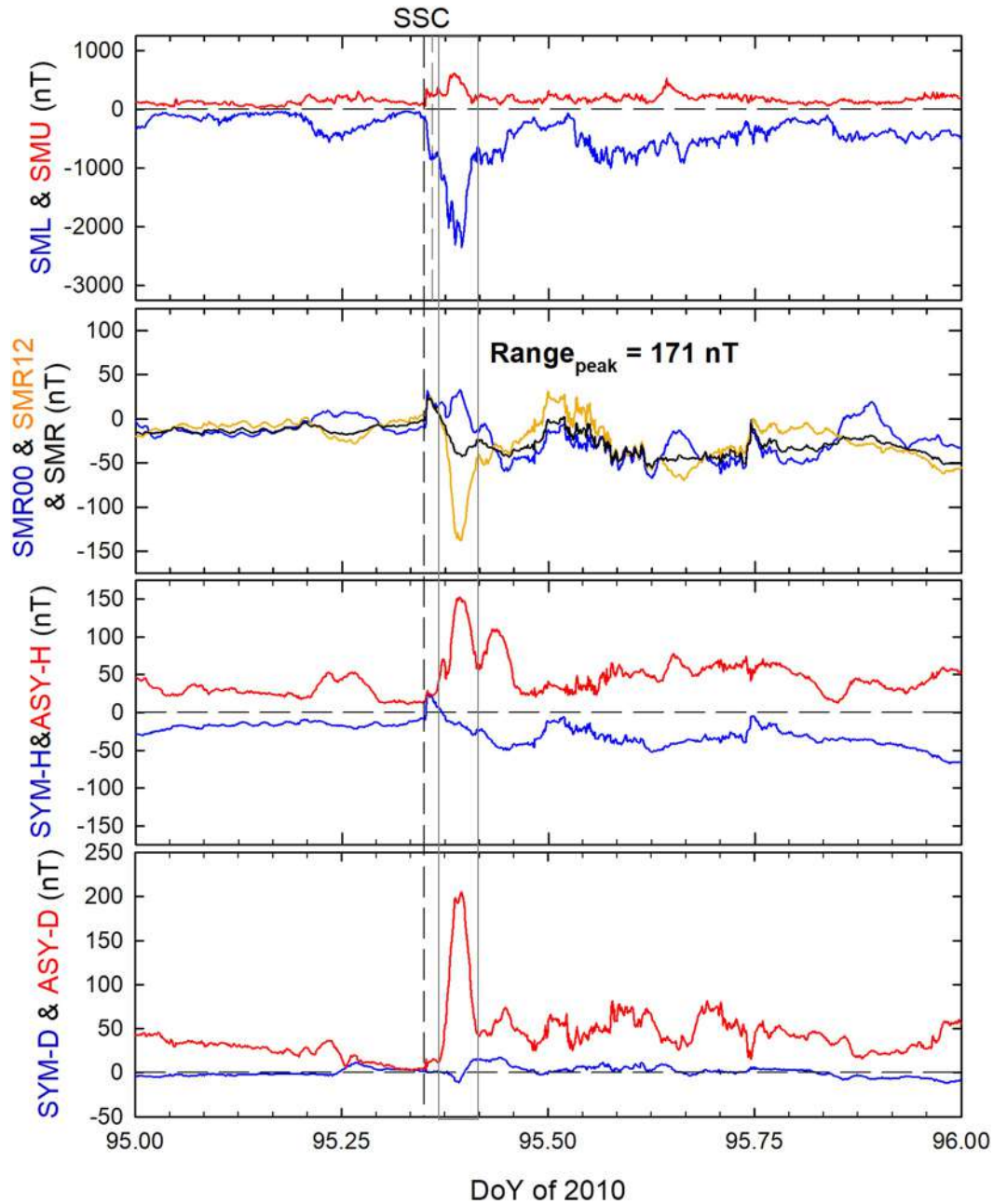

Figure A7. The event on 5 April 2010 (event #11 in Table 2). The format is the same as the one in the Figure A1.

Data Availability Statement

SuperMAG is an international collaboration with many organizations and institutes, and it is funded by National Science Foundation (NSF). The SML, SMU, SMR-12, and SMR-00 and SMR indices data were retrieved from the SuperMAG website (at https://supermag.jhuapl.edu/indices/); the SYM and ASY indices from the GSFC/SPDF OMNIWeb (at https://omniweb.gsfc.nasa.gov/form/omni_min.html); the Dst data were obtained through the Kyoto WDC (at http://wdc.kugi.kyoto-u.ac.jp/); the SSC data stem from the International Service of Geomagnetic Indices (at http://www.obsebre.es/en/rapid); Newell and Gjerloev (2011a, 2011b), Forsyth et al. (2015), Ohtani and Gjerloev (2020) substorm lists from the SuperMAG website (at https://supermag.jhuapl.edu/substorms/); the McMPB onset list from the supporting information (Data Set S4) of McPherron and Chu (2018).

Acknowledgments
This work was supported by the projects PID2020-119407GB-I00 and EPU-INV-UAH/2021/005. We thank one anonymous reviewer and the reviewer M. Hapgood for their helpful comments and advise to address future work. We gratefully acknowledge the SuperMAG collaborators (https://supermag.jhuapl.edu/info/?page=acknowledgement) and the SuperMAG team for their services.

References

Akasofu, S.-I. (1964). The development of the auroral substorm. *Planetary and Space Science*, *12*(4), 273–282. https://doi.org/10.1016/0032-0633(64)90151-5

Akasofu, S.-I., & Chapman, S. (1964). On the asymmetric development of magnetic storm fields in low and middle latitudes. *Planetary and Space Science*, *12*(6), 607–626. https://doi.org/10.1016/0032-0633(64)90008-X

Angelopoulos, V. (2008). The themis mission. *Space Science Reviews*, *141*(1), 5–34. https://doi.org/10.1007/S11214-008-9336-1

Borovsky, J. E., & Yakymenko, K. (2017). Substorm occurrence rates, substorm recurrence times, and solar wind structure. *Journal of Geophysical Research: Space Physics*, *122*(3), 2973–2998. https://doi.org/10.1002/2016JA023625

Boteler, D. H. (2019). A 21st century view of the March 1989 magnetic storm. *Space Weather*, *17*(10), 1427–1441. https://doi.org/10.1029/2019SW002278

Burch, J., Moore, T., Torbert, R., & Giles, B. L. (2016). Magnetospheric multiscale overview and science objectives. *Space Science Reviews*, *199*(1), 5–21. https://doi.org/10.1007/s11214-015-0164-9

Cid, C., Palacios, J., Saiz, E., Guerrero, A., & Cerrato, Y. (2014). On extreme geomagnetic storms. *Journal of Space Weather and Space Climate*, *4*, A28. https://doi.org/10.1051/swsc/2014026

Cid, C., Saiz, E., Guerrero, A., Palacios, J., & Cerrato, Y. (2015). A Carrington-like geomagnetic storm observed in the 21st century. *Journal of Space Weather and Space Climate*, *5*, A16. https://doi.org/10.1051/swsc/2015017

Clauer, C. R., & McPherron, R. L. (1980). The relative importance of the interplanetary electric field and magnetospheric substorms on partial ring current development. *Journal of Geophysical Research*, *85*(A12), 6747–6759. https://doi.org/10.1029/JA085iA12p06747

Coxon, J. C., Milan, S. E., Clausen, L. B. N., Anderson, B. J., & Korth, H. (2014). The magnitudes of the regions 1 and 2 Birkeland currents observed by ampere and their role in solar wind-magnetosphere-ionosphere coupling. *Journal of Geophysical Research: Space Physics*, *119*(12), 9804–9815. https://doi.org/10.1002/2014JA020138

Crooker, N. U. (1972). High-time resolution of the low-latitude asymmetric disturbance in the geomagnetic field. *Journal of Geophysical Research*, *77*(4), 773–775. https://doi.org/10.1029/JA077i004p00773

Davis, T. N., & Sugiura, M. (1966). Auroral electrojet activity index ae and its universal time variations. *Journal of Geophysical Research*, *71*(3), 785–801. https://doi.org/10.1029/JZ071i003p00785

Echer, E., Gonzalez, W. D., & Tsurutani, B. T. (2008). Interplanetary conditions leading to superintense geomagnetic storms (Dst ≤ -250 nT) during solar cycle 23. *Geophysical Research Letters*, *35*(6), L06S03. https://doi.org/10.1029/2007GL031755

Escoubet, C. P., Fehringer, M., & Goldstein, M. (2001). Introduction: The cluster mission. *Annales Geophysicae*, *19*(10/12), 1197–1200. https://doi.org/10.5194/angeo-19-1197-2001

Falayi, E. O., Ogunmodimub, A. O., Bolajic, O. S., Ayandaa, J. D., & Ojoniyi, O. S. (2017). Investigation of geomagnetic induced current at high latitude during the storm-time variation. *NRIAG Journal of Astronomy and Geophysics*, *6*(1), 131–140. https://doi.org/10.1016/j.nrjag.2017.04.010

Forsyth, C., Rae, I. J., Coxon, J. C., Freeman, M. P., Jackman, C. M., Gjerloev, J., & Fazakerley, A. N. (2015). A new technique for determining substorm onsets and phases from indices of the electrojet (sophie). *Journal of Geophysical Research: Space Physics*, *120*(12), 10592–10606. https://doi.org/10.1002/2015JA021343

Friis-Christensen, E., Lühr, H., & Hulot, G. (2006). Swarm: A constellation to study the Earth's magnetic field. *Earth Planets and Space*, *58*(4), 351–358. https://doi.org/10.1186/BF03351933

Fukushima, N., & Kamide, Y. (1973). Partial ring current models for worldwide geomagnetic disturbances. *Reviews of Geophysics*, *11*(4), 795–853. https://doi.org/10.1029/RG011i004p00795

Ganushkina, N. Y., Liemohn, M. W., & Dubyagin, S. (2018). Current systems in the earth's magnetosphere. *Reviews of Geophysics*, *56*(2), 309–332. https://doi.org/10.1002/2017RG000590

Ganushkina, N. Y., Liemohn, M. W., Dubyagin, S., Daglis, I. A., Dandouras, I., De Zeeuw, D. L., et al. (2015). Defining and resolving current systems in geospace. *Annales Geophysicae*, *33*(11), 1369–1402. https://doi.org/10.5194/angeo-33-1369-2015

Gaunt, C. T., & Coetzee, G. J. (2007). Transformer failures in regions incorrectly considered to have low GIC-risk. In *2007 IEEE Lausanne Power Tech* (pp. 807–812).

Gjerloev, J. W. (2012). The SuperMAG data processing technique. *Journal of Geophysical Research*, *117*(A9), 9213. https://doi.org/10.1029/2012JA017683

Gonzalez, W. D., Joselyn, J. A., Kamide, Y., Kroehl, H. W., Rostoker, G., Tsurutani, B. T., & Vasyliunas, V. M. (1994). What is a geomagnetic storm? *Journal of Geophysical Research*, *99*(A4), 5771–5792. https://doi.org/10.1029/93JA02867

Hajra, R., Tsurutani, B. T., Echer, E., Gonzalez, W. D., & Gjerloev, J. W. (2016). Supersubstorms (SML < -2500 nT): Magnetic storm and solar cycle dependencies. *Journal of Geophysical Research: Space Physics*, *121*(8), 7805–7816. https://doi.org/10.1002/2015JA021835

Harel, M., Wolf, R. A., Spiro, R. W., Reiff, P. H., Chen, C. K., Burke, W. J., et al. (1981). Quantitative simulation of a magnetospheric substorm 2. Comparison with observations. *Journal of Geophysical Research*, *86*(A4), 2242–2260. https://doi.org/10.1029/JA086iA04p02242

Iijima, T., & Potemra, T. A. (1976). Field-aligned currents in the dayside cusp observed by triad. *Journal of Geophysical Research*, *81*(34), 5971–5979. https://doi.org/10.1029/JA081i034p05971

Iyemori, T. (1990). Storm-time magnetospheric currents inferred from mid-latitude geomagnetic field variations. *Journal of Geomagnetism and Geoelectricity*, *42*(11), 1249–1265. https://doi.org/10.5636/jgg.42.1249

Iyemori, T., Araki, T., Kamei, T., & Takeda, M. (1992). *Mid-latitude geomagnetic indices ASY and SYM (provisional) no. 1 (1989–1990). Internal report of data analysis center for geomagnetism and space magnetism*. Kyoto University. Retrieved from https://wdc.kugi.kyoto-u.ac.jp/aeasy/asy.pdf

Iyemori, T., & Rao, D. (1996). Decay of the Dst field of geomagnetic disturbance after substorm onset and its implication to storm-substorm relation. *Annales Geophysicae*, *14*(6), 608–618. https://doi.org/10.1007/s00585-996-0608-3

Iyemori, T., Takeda, M., Nose, M., Odagi, Y., & Toh, H. (2010). Mid-latitude geomagnetic indices ASY and SYM for 2009 (provisional). In *Internal report of data analysis center for geomagnetism and space magnetism*. Kyoto University. Retrieved from https://wdc.kugi.kyoto-u.ac.jp/aeasy/asy.pdf

Kamide, Y., & Fukushima, N. (1972). Positive geomagnetic bays in evening high-latitudes and their possible connection with partial ring current. In *Report of Ionosphere and Space Research in Japan* (Vol. 26, pp. 79–101).

Kepko, L., McPherron, R. L., Amm, O., Apatenkov, S., Baumjohann, W., Birn, J., et al. (2015). Substorm current wedge revisited. *Space Science Reviews*, *190*(13), 1–46. https://doi.org/10.1007/s11214-014-0124-9

Kikuchi, T., Lühr, H., Schlegel, K., Tachihara, H., Shinohara, M., & Kitamura, T.-I. (2000). Penetration of auroral electric fields to the equator during a substorm. *Journal of Geophysical Research*, *105*(A10), 23251–23261. https://doi.org/10.1029/2000JA900016

Kikuchi, T., Tsunomura, S., Hashimoto, K., & Nozali, K. (2001). Field-aligned current effects on midlatitude geomagnetic sudden commencements. *Journal of Geophysical Research*, *106*(A8), 15555–15565. https://doi.org/10.1029/2001JA900030

Krafnät, S. (2011). Skydd mot geomagnetiska stormar elektromagnetisk. pa°verkan pa° kraftsystemet, Dnr, 805 (pp. 1–44). Retrieved from https://www.svk.se/siteassets/om-oss/rapporter/2015-och-aldre/120330-skydd-mot-geomagnetiska-stormar.pdf

Liemohn, M. W., McCollough, J. P., Jordanova, V. K., Ngwira, C. M., Morley, S. K., Cid, C., et al. (2018). Model evaluation guidelines for geomagnetic index predictions. *Space Weather*, *16*(12), 2079–2102. https://doi.org/10.1029/2018SW002067

Liou, K., Newell, P. T., Sibeck, D. G., Meng, C.-I., Brittnacher, M., & Parks, G. (2001). Observation of IMF and seasonal effects in the location of auroral substorm onset. *Journal of Geophysical Research*, *106*(A4), 5799–5810. https://doi.org/10.1029/2000JA003001

Lukianova, R. (2003). Magnetospheric response to sudden changes in solar wind dynamic pressure inferred from polar cap index. *Journal of Geophysical Research*, *108*(A12), 1428. https://doi.org/10.1029/2002JA009790

McPherron, R. L., & Chu, X. (2017). The mid-latitude positive bay and the MPB index of substorm activity. *Space Science Reviews*, *206*(1–4), 91–122. https://doi.org/10.1007/s11214-016-0316-6

McPherron, R. L., & Chu, X. (2018). The midlatitude positive bay index and the statistics of substorm occurrence. *Journal of Geophysical Research: Space Physics*, *123*(4), 2831–2850. https://doi.org/10.1002/2017JA024766

McPherron, R. L., Russell, C. T., & Aubry, M. P. (1973). Satellite studies of magnetospheric substorms on August 15, 1968: 9. Phenomenological model for substorms. *Journal of Geophysical Research*, *78*(16), 3131–3149. https://doi.org/10.1029/ja078i016p03131

Menvielle, M., Iyemori, T., Marchaudon, A., & Nose, M. (2010). Geomagnetic indices. *Geomagnetic Observations and Models*, *5*, 183–228. https://doi.org/10.1007/978-90-481-9858-0_8

Nahayo, E., Guerrero, A., Lotz, S., Cid, C., Tshisaphungo, M., & Saiz, E. (2022). Validating the LDi and LCi indices in the southern hemisphere. *Space Weather*, *20*(10), e2022SW003092. https://doi.org/10.1029/2022SW003092

Nakano, S., & Iyemori, T. (2005). Storm-time field-aligned currents on the nightside inferred from ground-based magnetic data at midlatitudes: Relationships with the interplanetary magnetic field and substorms. *Journal of Geophysical Research*, *110*(A7), A07216. https://doi.org/10.1029/2004JA010737

Newell, P. T., & Gjerloev, J. W. (2011a). Evaluation of SuperMAG auroral electrojet indices as indicators of substorms and auroral power. *Journal of Geophysical Research*, *116*(A12), A12232. https://doi.org/10.1029/2011JA016779

Newell, P. T., & Gjerloev, J. W. (2011b). Substorm and magnetosphere characteristic scales inferred from the SuperMAG auroral electrojet indices. *Journal of Geophysical Research*, *116*(A12), e2021JA029986. https://doi.org/10.1029/2011JA016936

Newell, P. T., & Gjerloev, J. W. (2012). SuperMAG-based partial ring current indices. *Journal of Geophysical Research*, *117*(A5), 5215. https://doi.org/10.1029/2012JA017586

Ngwira, C. M., & Pulkkinen, A. A. (2019). An introduction to geomagnetically induced currents. In *Geomagnetically induced currents from the sun to the power grid* (pp. 1–13). American Geophysical Union (AGU). https://doi.org/10.1002/9781119434412.ch1

Ohtani, S. (2022). New insights from the 2003 Halloween storm into the Colaba 1600 nt magnetic depression during the 1859 Carrington storm. *Journal of Geophysical Research: Space Physics*, *127*(9), e2022JA030596. https://doi.org/10.1029/2022JA030596

Ohtani, S., & Gjerloev, J. W. (2020). Is the substorm current wedge an ensemble of wedgelets?: Revisit to midlatitude positive bays. *Journal of Geophysical Research: Space Physics*, *125*(9), e2020JA027902. https://doi.org/10.1029/2020JA027902

Ohtani, S., Gjerloev, J. W., Anderson, B. J., Kataoka, R., Troshichev, O., & Watari, S. (2018). Dawnside wedge current system formed during intense geomagnetic storms. *Journal of Geophysical Research: Space Physics*, *123*(11), 9093–9109. https://doi.org/10.1029/2018JA025678

Ohtani, S., Imajo, S., Nakamizo, A., & Gjerloev, J. W. (2021). Globally correlated ground magnetic disturbances during substorms. *Journal of Geophysical Research: Space Physics*, *126*(4), e2020JA028599. https://doi.org/10.1029/2020JA028599

Østgaard, N., Tsyganenko, N. A., Mende, S. B., Frey, H. U., Immel, T. J., Fillingim, M., & Sigwarth, J. B. (2005). Observations and model predictions of substorm auroral asymmetries in the conjugate hemispheres. *Geophysical Research Letters*, *32*(5), L05111. https://doi.org/10.1029/2004GL022166

Pulkkinen, A., Lindahl, S., Viljanen, A., & Pirjola, R. (2005). Geomagnetic storm of 29–31 October 2003: Geomagnetically induced currents and their relation to problems in the Swedish high-voltage power transmission system. *Space Weather*, *3*(8), S08C03. https://doi.org/10.1029/2004SW000123

Pytte, T., McPherron, R., & Kokubun, S. (1976). The ground signatures of the expansion phase during multiple onset substorms. *Planetary and Space Science*, *24*(12), 1115-IN4. https://doi.org/10.1016/0032-0633(76)90149-5

Reddy, C., Kumar, S., & Somayajulu, V. (1988). An observational test for the ionospheric or magnetospheric origin of night-time geomagnetic positive bays at low and mid latitudes. *Planetary and Space Science*, *36*(11), 1149–1154. https://doi.org/10.1016/0032-0633(88)90069-4

Rostoker, G., Akasofu, S.-I., Foster, J., Greenwald, R., Kamide, Y., Kawasaki, K., et al. (1980). Magnetospheric substorms—Definition and signatures. *Journal of Geophysical Research*, *85*(A4), 1663–1668. https://doi.org/10.1029/JA085iA04p01663

Saiz, E., Cid, C., & Guerrero, A. (2021). The relevance of local magnetic records when using extreme space weather events as benchmarks. *Journal of Space Weather and Space Climate*, *11*, 35. https://doi.org/10.1051/swsc/2021018

Saiz, E., Guerrero, A., Cid, C., Palacios, J., & Cerrato, Y. (2016). Searching for Carrington-like events and their signatures and triggers. *Journal of Space Weather and Space Climate*, *6*, A6. https://doi.org/10.1051/swsc/2016001

Sastri, J. H., Rao, J. V. S. V., Rao, D. R. K., & Pathan, B. M. (2001). Daytime equatorial geomagnetic H field response to the growth phase and expansion phase onset of isolated substorms: Case studies and their implications. *Journal of Geophysical Research*, *106*(A12), 29925–29933. https://doi.org/10.1029/2001JA900120

Schillings, A., Palin, L., Opgenoorth, H. J., Hamrin, M., Rosenqvist, L., Gjerloev, J. W., et al. (2022). Distribution and occurrence frequency of *db/dt* spikes during magnetic storms 1980–2020. *Space Weather*, *20*(5), e2021SW002953. https://doi.org/10.1029/2021SW002953

Shi, Y., Zesta, E., & Lyons, L. R. (2008). Modeling magnetospheric current response to solar wind dynamic pressure enhancements during magnetic storms: 2. Application to different storm phases. *Journal of Geophysical Research*, *113*(A10), A10218. https://doi.org/10.1029/2008JA013420

Shi, Y., Zesta, E., Lyons, L. R., Yumoto, K., & Kitamura, K. (2006). Statistical study of effect of solar wind dynamic pressure enhancements on dawn-to-dusk ring current asymmetry. *Journal of Geophysical Research*, *111*(A10), A10216. https://doi.org/10.1029/2005JA011532

Siscoe, G. L., Lotko, W., & Sonnerup, B. U. (1991). A high-latitude, low-latitude boundary layer model of the convection current system. *Journal of Geophysical Research*, *96*(A3), 3487–3495. https://doi.org/10.1029/90JA02362

Sugiura, M. (1964). Hourly values of equatorial Dst for the IGY. In *Annals of the international geophysical year* (Vol. 35).

Sugiura, M., & Chapman, S. (1960). The average morphology of geomagnetic storms with sudden commencement. In *Contributions of the geophysical institute. Series B (University of Alaska, College), No. 50*. University of Alaska, Geophysical Institute.

Sun, W., Ahn, B.-H., Akasofu, S.-I., & Kamide, Y. (1984). A comparison of the observed mid-latitude magnetic disturbance fields with those reproduced from the high-latitude modeling current system. *Journal of Geophysical Research*, *89*(A12), 10881–10889. https://doi.org/10.1029/JA089iA12p10881

Tanskanen, E. I., Pulkkinen, T. I., Viljanen, A., Mursula, K., Partamies, N., & Slavin, J. A. (2011). From space weather toward space climate time scales: Substorm analysis from 1993 to 2008. *Journal of Geophysical Research*, *116*(A5), A00I34. https://doi.org/10.1029/2010JA015788

Tanskanen, E. I., Slavin, J. A., Tanskanen, A. J., Viljanen, A., Pulkkinen, T. I., Koskinen, H. E. J., & Eastwood, J. (2005). Magnetospheric substorms are strongly modulated by interplanetary high-speed streams. *Geophysical Research Letters*, *32*(16), L16104. https://doi.org/10.1029/2005GL023318

Thomson, A. W. P., Gaunt, C. T., Cilliers, P., Wild, J. A., Opperman, B., McKinnell, L.-A., et al. (2010). Present day challenges in understanding the geomagnetic hazard to national power grids. *Advances in Space Research*, *45*(9), 1182–1190. https://doi.org/10.1016/j.asr.2009.11.023

Trichtchenko, L., Boteler, D., & Boteler, D. (2004). Modeling geomagnetically induced currents using geomagnetic indices and data. *IEEE Transactions on Plasma Science*, *32*(4), 1459–1467. https://doi.org/10.1109/TPS.2004.830993

Tsurutani, B., & Hajra, R. (2021). The interplanetary and magnetospheric causes of geomagnetically induced currents (GICS) > 10 a in the Mäntsälä Finland pipeline: 1999 through 2019. *Journal of Space Weather and Space Climate*, *11*, 23. https://doi.org/10.1051/swsc/2021001

Tsurutani, B., Hajra, R., Echer, E., & Gjerloev, J. W. (2015). Extremely intense (SML ≤−2500 nt) substorms: Isolated events that are externally triggered? *Annales Geophysicae*, *33*(5), 519–524. https://doi.org/10.5194/angeo-33-519-2015

Untiedt, J., & Baumjohann, W. (1993). Studies of polar current systems using the IMS Scandinavian magnetometer array. *Space Science Reviews*, *63*(3–4), 245–390. https://doi.org/10.1007/BF00750770

Viljanen, A. (1997). The relation between geomagnetic variations and their time derivatives and implications for estimation of induction risks. *Geophysical Research Letters*, *24*(6), 631–634. https://doi.org/10.1029/97GL00538

Viljanen, A., Amm, O., & Pirjola, R. (1999). Modeling geomagnetically induced currents during different ionospheric situations. *Journal of Geophysical Research*, *104*(A12), 28059–28071. https://doi.org/10.1029/1999JA900337

Wik, M., Pirjola, R., Lundstedt, H., Viljanen, A., Wintoft, P., & Pulkkinen, A. (2009). Space weather events in July 1982 and October 2003 and the effects of geomagnetically induced currents on Swedish technical systems. *Annales Geophysicae*, *27*(4), 1775–1787. https://doi.org/10.5194/angeo-27-1775-2009

Yamauchi, M., Iyemori, T., Frey, H., & Henderson, M. (2006). Unusually quick development of a 4000 nt substorm during the initial 10 min of the 29 October 2003 magnetic storm. *Journal of Geophysical Research*, *111*(A4), A04217. https://doi.org/10.1029/2005JA011285

Zhang, J. J., Yu, Y. Q., Chen, W. Q., Wang, C., Liu, Y. D., Liu, C. M., & Liu, L. G. (2022). Simulation of geomagnetically induced currents in a low-latitude 500 kv power network during a solar superstorm. *Space Weather*, *20*(4), e2021SW003005. https://doi.org/10.1029/2021SW003005